

1 **Circulating immune complexes drive immunopathology in COVID-19**

2 Jakob Ankerhold^{1*}, Sebastian Giese^{1*}, Philipp Kolb^{1*}, Andrea Maul-Pavicic², Nathalie
3 Göppert¹, Kevin Ciminski¹, Clemens Kreuzt⁴, Achim Lothar^{5,6}, Ulrich Salzer³, Wolfgang
4 Bildl⁷, Tim Welsink⁸, Nils G. Morgenthaler⁸, Andrea Busse Grawitz⁹, Daniela Huzly¹, Martin
5 Schwemmle¹, Hartmut Hengel^{1§}, Valeria Falcone^{1§}

6
7 ¹Institute of Virology, Freiburg University Medical Center, Faculty of Medicine, Albert-
8 Ludwigs-University of Freiburg, Freiburg, Germany.

9 ²Department of Rheumatology and Clinical Immunology, Freiburg University Medical Center,
10 Faculty of Medicine, Albert-Ludwigs-University of Freiburg, Freiburg, Germany.

11 ³Center for Chronic Immunodeficiency (CCI), Freiburg University Medical Center, Faculty of
12 Medicine, Albert-Ludwigs-University of Freiburg, Freiburg, Germany.

13 ⁴Institute of Medical Biometry and Statistics, Freiburg University Medical Center, Faculty of
14 Medicine, Albert-Ludwigs-University of Freiburg, Freiburg, Germany.

15 ⁵Heart Center Freiburg University, Department of Cardiology and Angiology I, Faculty of
16 Medicine, Albert-Ludwigs-University of Freiburg, Freiburg, Germany.

17 ⁶Institute of Experimental and Clinical Pharmacology and Toxicology, Faculty of Medicine,
18 Albert-Ludwigs-University of Freiburg, Freiburg, Germany.

19 ⁷Institute of Physiology II, Faculty of Medicine, Albert-Ludwigs-University of Freiburg,
20 Freiburg, Germany.

21 ⁸InVivo BioTech Services GmbH, Hennigsdorf, Germany.

22 ⁹Institute of Clinical Chemistry and Laboratory Medicine, Faculty of Medicine, Albert-
23 Ludwigs-University of Freiburg, Freiburg, Germany.

24

25 * contributed equally

26 § corresponding authors

27

28 Email: Hartmut.hengel@uniklinik-freiburg.de; valeria.kapper-falcone@uniklinik-freiburg.de

29

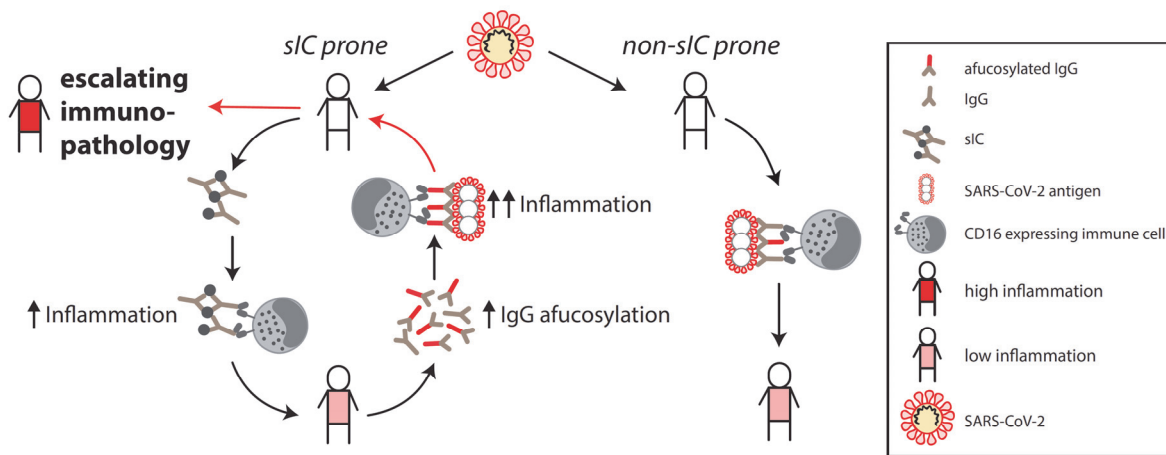
30

31 **Conflict of interest**

32 The authors declare the following competing financial interest(s): InVivo BioTech Services is
33 a biotechnology company producing antibodies and proteins, including SARS-CoV-2 antigens.

34

35 Graphical abstract



36
37

38 **Model: A vicious cycle of immunopathology in COVID-19 patients is driven by soluble**
39 **multimeric immune complexes (sICs).** SARS-CoV-2 infection triggers sIC formation in
40 prone individuals. Activation of Fc γ RIII/CD16 expressing immune cells by sICs precedes a
41 humoral response to SARS-CoV2 infection. sICs and infection add to IgG afucosylation, further
42 enhancing Fc γ RIII/CD16 activation by opsonized targets. High inflammation induces further
43 sIC mediated immune cell activation ultimately leading to an escalating immunopathology.
44

44

45

46 Abstract

47 A dysregulated immune response with high levels of SARS-CoV-2 specific IgG antibodies
48 characterizes patients with severe or critical COVID-19. Although a robust IgG response is
49 traditionally considered to be protective, excessive triggering of activating Fc-gamma-receptors
50 (Fc γ Rs) could be detrimental and cause immunopathology. Here, we document that patients
51 who develop soluble circulating IgG immune complexes (sICs) during infection are subject to
52 enhanced immunopathology driven by Fc γ R activation. Utilizing cell-based reporter systems
53 we provide evidence that sICs are predominantly formed prior to a specific humoral response
54 against SARS-CoV-2. sIC formation, together with increased afucosylation of SARS-CoV-2
55 specific IgG eventually leads to an enhanced CD16 (Fc γ RIII) activation of immune cells. Our
56 data suggest a vicious cycle of escalating immunopathology driven by an early formation of
57 sICs in predisposed patients. These findings reconcile the seemingly paradoxical findings of
58 high antiviral IgG responses and systemic immune dysregulation in severe COVID-19.
59

59

60

61 Introduction

62

63 Since the emergence of SARS-CoV-2 in late December 2019¹, more than 197 million laboratory
64 confirmed infections (as of July 31, 2021) have been reported, with cases continuously rising².
65 Accordingly, rapid insights into the disease manifestations and pathogenesis have been globally
66 obtained. A hallmark of the coronavirus disease 2019 (COVID-19) is a respiratory infection
67 which can progress to an acute respiratory distress syndrome (ARDS). Next to asymptomatic
68 infections, COVID-19 symptoms differ widely according to the disease process and may
69 comprise fever, coughing, pneumonia, dyspnea, hypoxia and lymphopenia³. While fever and
70 coughing are common symptoms, pneumonia, hypoxia, dyspnea, certain organ manifestations
71 and lymphopenia indicate critical or fatal infections³⁻⁶. Pronounced dyspnea can eventually
72 progress to ARDS, a severe complication frequently observed in critically ill patients^{7,8}.
73 Although overall disease severity and in particular breathing difficulties are related to viral
74 load⁹, age^{4,10-13} and underlying medical conditions^{4,11,12}, the delayed kinetics of respiratory
75 failure strongly suggest an essential role of the host immune response^{3,11}. Typically, aggravation
76 occurs between 9-12 days after symptom onset¹² and correlates with high levels of SARS-CoV-
77 2 specific IgG antibodies and systemic effects of pro-inflammatory cytokines such as IL-6 and
78 TNF α ^{3,14-16}. This cytokine release, primarily the result of macrophage and T helper (T_H) cell
79 activation¹⁷, includes pattern recognition receptor (PRR) signaling in the context of innate
80 immunity but can also occur by Fc γ receptor (Fc γ R) activation¹⁸. Triggered by immune
81 complexes (antibody-antigen complex), the cytokine release following Fc γ R activation
82 represents a potent defense mechanism against invading pathogens. A prototypical activating
83 Fc γ R in this regard is Fc γ RIII (CD16) expressed by NK cells^{19,20}, monocyte-derived
84 macrophages (CD16A)²¹ or neutrophils (CD16B, 98% sequence identical ectodomains).
85 Specifically, CD16 is able to sense circulating soluble immune complexes (sICs) as they are
86 formed in certain autoimmune diseases such as lupus²²⁻²⁵ and viral infections²⁶. Overstimulation
87 of activating Fc γ Rs in these cases is associated with disease severity²⁶⁻²⁸ and thus an Fc γ R-
88 driven overshooting inflammatory response¹⁸ might be an explanation for the pronounced
89 immunopathology observed during severe courses of COVID-19²⁹. Consistently, hyper-
90 inflammation in SARS-CoV-1 and MERS infected patients has been previously proposed as a
91 possible pathogenic factor³⁰ and could be demonstrated in mice and macaques infected with
92 SARS-CoV-1^{31,32}. Furthermore, N297-dependent glycan-modifications such as afucosylation
93 within the constant region of SARS-CoV-2 specific IgG antibodies should enhance binding to
94 Fc γ Rs, in turn driving inflammation. Enhanced Fc γ RIII activation by low-fucosylated anti-
95 SARS-CoV-2-S IgG leading to excessive alveolar macrophage activation has specifically been
96 shown to drive severe COVID-19 disease progression³³. Therefore we aimed to delineate the
97 contribution of IgG-mediated effector functions regarding COVID-19 severity in patient
98 cohorts with various severity of SARS-CoV-2 infection. This revealed a marked correlation
99 between CD16 activation by patient IgG and severity of disease. Additionally, we identified
100 circulating CD16-reactive sICs to be abundantly present in the serum of patients with critical
101 and severe disease, but not in the serum of those with a mild disease. As sIC formation preceded
102 a SARS-CoV-2 specific humoral response in most cases, we conclude that a so far undisclosed
103 predisposing condition divides patients into sIC-prone and non-sIC-prone individuals with
104 patients developing sICs in response to an infectious trigger also developing enhanced disease.
105 Our data suggest a vicious cycle leading to an escalating immunopathology driven by the early
106 formation of sICs. Our findings enable new avenues of intervention against COVID-19 and
107 highly warrant further investigation into the origin and composition of sICs predisposing to
108 COVID-19 disease.

109

110 **Results**

111

112 **Patients and clinical information.**

113 We retrospectively analyzed serial serum samples collected for routine diagnostic testing from
114 41 patients hospitalized at our tertiary care center between March and June 2020 with SARS-
115 CoV-2 infection confirmed by real-time PCR. Based on the clinical course, we categorized
116 patients as either severely diseased (hospitalized with COVID-19 related pneumonia) versus
117 critically diseased (COVID-19 related pneumonia and eventually in need of invasive
118 mechanical ventilation). In total, 27 patients with critical and 14 with severe courses of disease
119 were grouped into separate cohorts (Table 1). Most patients were older than 60 years with an
120 overall mean age of 68 years (63 years and 76 years in the critically and severely diseased
121 patients respectively). The majority of patients in both groups had comorbidities of different
122 origin with cardiovascular diseases including hypertension representing the most frequent
123 pathology (35/41, 85%). Similar to previous reports, high Interleukin 6 (IL-6) and C-reactive
124 protein (CRP) levels were associated with severity of disease ($\bar{\text{IL-6}}$: 1452.1 pg/ml in the
125 critical group vs 46.1 pg/ml in the severe group and $\bar{\text{CRP}}$: 162.2 mg/l vs 65.3 mg/l, $\bar{\text{IL-6}}$ 13-25
126 days post symptom onset respectively). Similarly, procalcitonin, a biomarker of microbial
127 coinfection, was significantly higher in critically diseased patients ($\bar{\text{value}}$ 9.9 ng/ml vs 0.17
128 ng/ml). Bacterial superinfection represented a further complication in 39% of the patients and
129 was only slightly more frequent in patients with critical disease (11/27, 41% vs 5/14, 33%).
130 More than half of the patients (59%) were treated with hydroxychloroquine/Lopinavir and
131 Ritonavir (Kaletra®), (18/27, 67% in the critical group vs 6/14, 43% in the severe group).
132 Notably, at the time of serum acquisition, only one patient received steroid treatment, which
133 was given due to underlying chronic obstructive pulmonary disease. Finally, mortality rate was
134 37% (10/27) in critically and 7% (1/14) in severely diseased patients.

135

136 **Kinetics of IgG antibody responses following symptom onset across severe and critical** 137 **courses of disease.**

138 It has been observed that elevated SARS-CoV-2 antibody titers are associated with disease
139 severity¹⁵ and speculated to play a role not only in the clearance but also in the pathogenesis of
140 SARS-CoV-2 infection³⁴. We initially analyzed the levels and kinetics of SARS-CoV-2 specific
141 IgG in serial serum samples from patients hospitalized with critical (n=27) or severe (n=14)
142 illness, a setting we also used in the following experiments. A total of 125 (critically diseased)
143 and 79 (severely diseased) serum samples, obtained from the aforementioned patients at
144 different time points within 6-25 days following symptom onset were analyzed by
145 commercially available S1- and N- specific ELISA-based assays. Assay specificity was
146 confirmed analyzing healthy donor (HD) serum samples (n=30) as negative control (Figure 1-
147 figure supplement 1 A, B). Most patients developed detectable SARS-CoV-2 specific IgG
148 responses within 9-14 days after symptom onset. SARS-CoV-2 specific IgG gradually
149 increased over time in both severely and critically diseased patients reaching a plateau at 18-20
150 days after symptom onset (Figure 1 A, B). Varying antibody response kinetics were observed
151 for each individual patient (Figure 1-figure supplement 2 A-D) with anti-N IgG titers rising
152 significantly earlier than anti-S1 IgG (12.5 days \pm 3.3 days vs 10.6 \pm 3.8; p = 0.0091). A trend
153 towards earlier seroconversion for anti-S1 IgG could be observed in critically diseased patients
154 (mean time of seroconversion 11.4 \pm 3.0 days in critically diseased patients vs 12.9 \pm 3.8 days
155 for severely diseased patients; p = 0.24), whereas time of seroconversion for anti-N IgG was
156 similar in both groups (10.1 \pm 3.2 and 10.4 \pm 4.2 days for critically and severely diseased
157 patients, respectively; p = 0.83). S1- and N-specific IgG levels at plateau did not significantly
158 differ between the two groups. No significant difference between deceased and discharged
159 patients was measured 13-25 days after symptom onset (Figure 1- figure supplement 1 C, D,
160 E). Next, we evaluated and compared the neutralizing capacity of SARS-CoV-2 antibodies in

161 either critically versus severely diseased patients in a plaque-reduction assay (Figure 1 C). All
162 patients mounted a robust neutralizing antibody response ($91\% \pm 10.5\%$ neutralization at a
163 1:64 serum dilution), with peaking titers at 18-20 days following symptom onset. Of note, two
164 critically diseased patients developed a neutralizing response already at 6-8 days after symptom
165 onset. In summary, we observed only minor differences in cohort wide kinetics of S1- or N-
166 specific IgG levels between patients hospitalized with severe or critical clinical courses
167 indicating that antibody levels per se did not correlate with severity of disease in our study.

168

169 **Patients with severe COVID 19 show enhanced Fc γ RIII/CD16 activation by S-specific IgG** 170 **antibodies.**

171 Fc γ RIII (CD16) activation initiates multiple protective effector functions such as antibody-
172 dependent cellular cytotoxicity (ADCC) by natural killer (NK) cells as well as antibody-
173 dependent cytokine and chemokine secretion by NK cells and macrophages^{18,35}. However,
174 excessive Fc γ R stimulation can have severe adverse effects such as elevated cytokine release
175 as observed in systemic autoimmune diseases or viral infections¹⁸. Therefore, we hypothesized
176 that an exaggerated Fc γ R mediated activation triggered by SARS-CoV-2 specific IgG might
177 contribute to the exacerbation of COVID-19 in severely compared to critically diseased
178 patients. To address this, we analyzed the ability of SARS-CoV-2 specific antibodies to activate
179 CD16 (158V) using a previously validated cell-based reporter system³⁶⁻⁴⁰ (Figure 2- figure
180 supplement 1A). Considering the typically late time point of health deterioration, we performed
181 an analysis of CD16 activation triggered by SARS-CoV-2 specific IgG with serum samples
182 obtained 13-25 days following symptom onset (Figure 2). Sera were analyzed at a 1:500
183 dilution to stay within the dynamic range of detection (Figure 2- figure supplement 2).
184 Depending on the availability of sample material 2-8 samples/patient/time-point were included
185 in this analysis. If available in sufficient quantity, sera were reanalyzed. Reproducibility was
186 tested using available serum surplus (Figure 2- figure supplement 3). Sera from 28 patients with
187 mild SARS-CoV-2 infection and 30 healthy blood donors were included for reference. Semi-
188 quantitative assessment of IgG titers using antigen-specific ELISA revealed comparable levels
189 between critically and severely diseased patient cohorts (Figure 2 A, B, C). In contrast, S-
190 ($p=0.0147$) and RBD-specific ($p=0.0120$) but not N-specific IgG-mediated CD16 activation
191 was significantly increased in critically compared to severely diseased patients (Figure 2 D-F).
192 Furthermore, normalizing CD16 activation to antigen-specific IgG titers, revealed significantly
193 stronger CD16 activation by S- ($p=0.0033$) and N-specific ($p=0.006$) IgG compared to mildly
194 diseased patients (Figure 2 G-I). Intriguingly, we observed a heterogeneous CD16 activation
195 pattern characterized by either high or low CD16-activating sera irrespective of the clinical
196 manifestation (Figure 2 D-F). Overall, a significant positive correlation could be determined
197 between anti-SARS-CoV-2 antigen IgG titers and CD16 activation (Figure 2-figure supplement
198 4). Our data document a sustained CD16 activation by SARS-CoV-2 specific antibodies
199 particularly in patients suffering from critical COVID-19 disease. Based on these results we
200 confirmed the notion that elevated Fc γ RIII/CD16 activation by S- and or RBD-specific IgG
201 might contribute to disease severity of COVID-19.

202

203 **Enhanced Fc γ -afucosylation of S-specific IgG in critically and severely diseased patients** 204 **results in increased Fc γ RIII/CD16 activation.**

205 Based on the findings described above we speculated that differences in Fc γ mediated effector
206 functions might contribute to disease severity of COVID-19. We compared CD16 high- versus
207 CD16 low-activating patient sera regarding their SARS-CoV-2 specific IgG core fucosylation.
208 Inspired by previous findings⁴¹⁻⁴³ we focused on determining IgG core fucosylation of S- and
209 N- specific SARS-CoV2 IgG. To determine IgG core fucosylation we used a lectin-based
210 ELISA preceded by antigen-specific antibody purification from immobilized SARS-CoV-2-
211 antigen. Analysis of anti-S and anti-N IgG core fucosylation was performed on serum pools

212 containing five sera of either critically or severely diseased patients obtained 13-25 days post
213 symptom onset. Given the aforementioned heterogeneity in CD16-activation, we analyzed
214 pools of 5 sera of either critically or severely diseased patients characterized by either high or
215 low CD16-activation. To stay within the dynamic detection range, relative fucosylation was
216 analyzed at a dilution of 1:4 (Figure 3). When analyzing serum pools from critically and
217 severely diseased patients we determined a significantly lower level of core fucosylation among
218 the high CD16 activators (Figure 3, plain-colored bars) compared to the low CD16 activators
219 (Figure 3, shaded bars). This applied for both the S- and N-specific antibodies. These results
220 are in line with previously published findings regarding the effect of Fc γ -afucosylation on
221 Fc γ RIII/CD16 effector functions^{41,44} and recapitulate similar findings in the context of COVID-
222 19^{42,43}. However, we did not observe significant differences between critically and severely
223 diseased patients.

224 225 **COVID-19 disease severity correlates with an increase in Fc γ RIII/CD16-reactive soluble** 226 **IgG complexes.**

227 Next to afucosylation, it has been proposed that uncleared antigen-antibody immune complexes
228 (ICs) might further exacerbate inflammation, explaining complications observed in COVID-19
229 such as cytokine storm, systemic vasculitis, microvascular thrombosis and organ failure⁴⁵⁻⁴⁷.
230 However, the presence of circulating, multimeric soluble ICs (sICs) in critically or severely
231 diseased patients has not been conclusively shown yet. As extensive Fc γ R activation by sICs
232 might contribute to the severe systemic inflammatory state occurring in some COVID-19
233 patients with prolonged disease, we surmised that sICs might be a putative explanation for the
234 marked differences in IL-6, PCT and CRP levels between critically and severely diseased
235 patients (Table 1). We thus set out to characterize our patient cohort regarding the presence of
236 sICs in serum samples taken at various time points during disease and after hospitalization. To
237 this end, we deployed a novel cell-based reporter assay developed to quantify CD16 (158V)
238 activation by IgG-containing sICs²⁵. As recently shown, the assay does not react to monomeric
239 IgG or small dimeric complexes in solution, but specifically identifies multimeric sICs and has
240 been successfully used to detect sICs in patients with systemic lupus erythematosus (SLE)
241 known to exhibit sICs²⁴. Moreover, the assay is sensitive to sICs size with larger complexes
242 leading to stronger receptor activation compared to small complexes²⁵. Analysis of serum
243 samples, obtained 13-25 days after symptom onset, revealed the presence of highly CD16-
244 reactive sICs in SARS-CoV-2 infected patients compared to healthy individuals (Figure 4A).
245 Next, we compared sIC-mediated CD16 activation between COVID-19 patients of varying
246 disease severity. While all COVID-19 patient groups tested positive for reactive sICs compared
247 to healthy control (HD) sera, we found that critically diseased patients show a striking increase
248 in reactive sICs compared to patients with severe or mild disease (Figure 4B). Only 6 out of 27
249 patients with critical disease (22%) showed no sIC-mediated CD16 activation. As we did not
250 detect highly reactive sICs in the serum of 47 patients with acute respiratory distress syndrome
251 (ARDS; mean age 57.5 years) in response to infections of different etiology including CMV
252 reactivation, HIV/AIDS, influenza or pulmonary TBC infection, we conclude that the formation
253 of reactive sICs is associated with severe SARS-CoV-2 disease (Figure 4-figure supplement 1).
254 Remarkably, longitudinal analysis of reactive sICs in the serum of critically or severely diseased
255 patients revealed high CD16 activation levels in 4 critically diseased patients already 6 to 8
256 days after symptom onset (Figure 4C). Of note, 2 of 4 patients with an early increase of
257 circulating reactive sIC eventually died. sIC-mediated CD16 activation persisted in 14 of 19
258 critically diseased patients at high levels until day 26 after symptom onset. sIC-mediated CD16
259 activation in severely diseased patients was slightly delayed compared to critically diseased
260 patients and was first detected in 4 patients 9-11 days after symptom onset (Figure 4C). Only 4
261 of 14 patients with severe disease showed detectable sIC-mediated CD16 activation. To verify
262 that sICs represent the CD16-reactive component in the serum of COVID-19 patients, we

263 analyzed serum-mediated CD16 activation before and after PEG8000-precipitation. This
264 treatment was previously shown to selectively precipitate large IgG complexes from
265 solution^{25,48}. For this analysis, pools of 8 sera, showing either high (IC+) or no (IC-) CD16
266 activation, were compared. Sera from healthy donors (HD) served as a negative control.
267 Compatible with the hypothesis of serum-derived sICs driving CD16 activation, no activation
268 was observed following incubation with 3.5% PEG8000 (Figure 4-figure supplement 2 A). To
269 ensure that the treatment did not precipitate monomeric IgG, we tested the depleted sera for
270 remaining S1- and N-specific IgG. As depicted S1- and N- specific IgG could still be detected
271 at unchanged high levels in samples treated with 3.5% PEG8000 (Figure 4-figure supplement
272 2 B). When resolving sIC-mediated CD16 activation over the complete time of hospitalization
273 for select patients from which samples at different time points were available, we observed that
274 sIC reactivity predominantly precedes anti-S1 IgG in ELISA as well as CD16 activation by
275 SARS-CoV-2-specific IgG (Fig. 4-figure supplement 3, Fig. 4-figure supplement 5). This
276 implies that sIC formation does not depend on the presence of SARS CoV-2 antigens.
277 Accordingly, we were not able to identify any SARS-CoV-2-derived antigens in PEG8000-
278 precipitated sICs using tandem mass spectrometry (data not shown). To further exclude the
279 formation of multimeric sICs formed from circulating S1 antigen, we also specifically targeted
280 S1 for precipitation from patient serum using biotinylated S1-specific monoclonal antibodies.
281 However and in line with our previous approach, S1-specific precipitation using streptavidin-
282 sepharose beads and subsequent mass spectrometry analysis for any SARS-CoV-2-specific
283 antigens in sICs remained without result (data not shown). Recently, the role of neutrophil
284 mediated intravascular NETosis was reported to play a critical role in thrombose formation and
285 subsequent organ damage observed in severe clinical forms of COVID-19⁴⁹⁻⁵¹. Since this
286 process could mediate the formation of aggregated IgG as a form of sICs, we next tested
287 whether Benzonase® nuclease treatment of patient serum would dissolve reactive sICs. To this
288 end we tested sera from critically diseased patients or healthy individuals and compared CD16
289 reactivity before and after nuclease treatment (Figure 4-figure supplement 4). Nuclease activity
290 in diluted human serum was controlled using plasmid DNA for reference. This revealed that
291 nucleic acid was not involved in the formation of CD16-reactive sICs in critically diseased
292 patients. Finally, we tested pooled patient sera for autoantibodies against a panel of prototypical
293 autoantigens associated with autoimmune disease including anti-nuclear autoantibodies (ANA)
294 by indirect immunofluorescence, dsDNA autoantibodies by ELISA and autoantibodies against
295 the extractable nuclear antigens (nRNP/Sm, Sm, SS-A, Ro-52, SS-B, Scl-70, PM-Scl, Jo-1,
296 CENP B, PCNA, nucleosomes, histones, ribosomal P-protein, AMA-M2, DFS70) by dot blot
297 in case SARS-CoV-2 infection triggers autoantibody formation and possible sIC formation.
298 However, no significant autoantibody titers could be detected in any sera pool (data not shown).
299 Although we were not able to identify their origin, our data clearly indicates the presence of
300 circulating sICs in COVID-19 patients with an increase in CD16-reactive sICs corresponding
301 with severity of disease. Accordingly, we conclude that circulating sICs are a hitherto unknown,
302 yet contributing factor to COVID-19 disease severity and, regarding infectious diseases, our
303 findings represent an observation unique to severely diseased COVID-19 patients.

304
305

306 Discussion

307

308 We collected and analyzed data from 41 COVID-19 patients hospitalized at the University
309 Hospital Freiburg. Patients were categorized by severity of disease into severely (n=14) and
310 critically diseased patients (n=27). Both groups were of comparable average age and had a
311 similar male-to-female ratio. For comparison we also analyzed 28 mildly diseased and 30
312 healthy individuals. As key findings we identify *de novo* produced afucosylated SARS-CoV-2

313 IgG and the presence of soluble immune complexes activating FcγRIII/CD16 as potential risk
314 factors closely associated with severe courses of COVID-19.

315

316 **FcγRIII/CD16 activation by SARS-CoV-2 specific IgG is increased in critically diseased**
317 **patients.** FcγR activation by anti-viral IgG represents a potent defense mechanism, directing
318 the immune response to the site of viral replication⁵²⁻⁵⁵. However, persistent infection can lead
319 to prolonged stimulation of FcγRs, driving an overshooting and potentially damaging
320 inflammatory response^{18,26}. A potential key component in prolonged inflammation following
321 SARS-CoV-2 infection is FcγR mediated cytokine and chemokine release by several immune
322 cells as their activation has been implied in severity of disease^{41,43,56}. Along these lines, glycan
323 profiles of anti-SARS-CoV-2 IgG have been identified as major correlates of COVID-19
324 disease progression⁴¹⁻⁴³. As these modifications particularly affect FcγRIII/CD16 receptor
325 triggering, we characterized our patient groups with regard to CD16 activation by S- and N-
326 specific IgG and determined significantly increased CD16 activation by S-, N- and RBD-
327 specific IgG in sera from severely and critically diseased patients compared to mildly diseased
328 patients. We further identified a higher level of afucosylation being indicative of COVID-19
329 severity, which is in line with previous studies⁴¹⁻⁴³, and now directly link this biochemical
330 feature to an increased CD16 receptor activation. Taken together, we find that CD16 triggering
331 by SARS-CoV-2-specific IgG can be directly correlated to IgG glycan modifications and
332 disease severity.

333

334 **Circulating sICs contribute to COVID-19 disease severity.**

335 Based on the herein presented results identifying FcγRIII/CD16 receptor activation to be a
336 major correlate of disease severity, we further explored this FcγR using an adapted reporter cell
337 activation assay optimized to measure sICs²⁵. Indeed, we provide first evidence of such
338 circulating sICs in the serum of COVID-19 patients and experimentally confirm previous
339 hypotheses suggesting immune complexes as potential drivers of disease progression in
340 COVID-19⁴⁵⁻⁴⁷. In fundamental contrast to opsonized antigens decorating virus-infected cells
341 in tissues, sICs become distributed systemically. Thus constitutive activation of CD16⁺
342 monocytes, granulocytes and NK cells could readily explain systemic responses which
343 potentiate local inflammation in virus-infected tissues intensifying organ damage and
344 dysfunction. Although the origin of the circulating immune complexes still remains elusive, we
345 clearly show that the presence of IgG-containing sICs during SARS-CoV-2 infection is directly
346 responsible and sufficient for the observed FcγRIII/CD16 activation by patient serum. As we
347 find sIC reactivity to predominantly precede SARS-CoV-2-S specific IgG responses, we
348 conclude that circulating S or shed S1-antigens are not involved in sIC formation. Although
349 sICs are commonly associated with immunopathology in autoimmunity^{23,24,57} and several
350 studies have described that certain auto-antibodies can be detected in certain critically ill
351 COVID-19 patients⁵⁸⁻⁶⁰, we could not identify a clear autoimmunity profile linked to sIC
352 formation when searching for prototypical autoantibodies. However, as sIC formation seems
353 to represent an intrinsic risk factor we classified patients as sIC-prone or non-sIC-prone
354 (graphical abstract). We suggest a hidden predisposition in sIC-prone patients resulting in a
355 strong early inflammatory response to SARS-CoV-2 infection possibly being a trigger for
356 further sIC formation and the generation of afucosylated SARS-CoV-2 IgG. Very recent work
357 reports that an acute SARS-CoV-2 infection triggers the *de novo* IgG production against
358 multiple autoantigens. In this study, 60-80% of all hospitalized COVID-19 patients exhibited
359 anti-cytokine IgG (ACA)⁶¹. The authors show that ACA levels and specificity change over time
360 during hospitalization, suggesting ACA induction in response to viral infection and
361 inflammation. Further, it has been shown that pre-existing neutralizing anti-type I interferon
362 antibodies, which can be found in about 10% of patients with severe COVID-19 pneumonia,
363 are related to the highest risk of developing life-threatening COVID-19 disease⁶². Therefore,

364 the *de novo* induction of anti-cytokine auto-antibodies in a large proportion of hospitalized
365 COVID-19 patients as described by Chang et al.⁶¹, might indeed represent a source of
366 circulating sICs in COVID-19. In such a scenario, immune responses are deviated first by an
367 immunodepletion of critical cytokines and second through the formation of pathological sICs
368 which trigger immunological damage. We show that critically diseased patients show
369 significantly higher levels of reactive sICs compared to less severely diseased patients. In
370 addition, sIC responses can be found significantly earlier in critically diseased patients, which
371 was associated with a fatal disease outcome. We also find that patients show a wide range of
372 sIC reactivity. According to the Heidelberger-Kendall precipitation curve⁶³, sIC size is critically
373 dependent on the antigen:antibody stoichiometry. As the used FcγR activation assay is highly
374 sensitive to sIC size²⁵, it is likely that this also plays a role when detecting this bioactivity in
375 COVID-19 patient serum. Therefore, we propose that in addition to the presence of sICs, the
376 size of sICs plays a role in CD16 driven COVID-19 immunopathology.
377 Taken together, we conclude that CD16 activation in COVID-19 disease is governed by sIC
378 formation and IgG glycan profiles (Figure 5), both playing a major role in disease progression
379 and severity. It can be hypothesized that the formation of sICs in predisposed patients initiates
380 a vicious circle of FcγR-mediated inflammation leading to an increase of IgG afucosylation,
381 followed by enhanced FcγR activation by SARS-CoV-2-specific IgG, further contributing to
382 inflammation and, conceivably, to *de-novo* sIC formation. Indeed, there is evidence in this
383 direction from a clinical perspective provided by a recent study that finds the administration of
384 intravenous immunoglobulin (IVIg) to alleviate COVID-19 disease⁶⁴. Although no direct proof,
385 this heavily implies that the saturation of FcγRs mitigates immunopathology as previously
386 reported for autoimmune diseases⁶⁵. Therefore, our findings provide an explanation for the
387 sustained immunopathology following SARS-CoV-2 infection observed in some patients as
388 well as for the efficacy of IVIg treatment in severe to critical COVID-19 disease. Finally, it will
389 be important to investigate whether sICs observed in severely diseased COVID-19 patients may
390 persist after resolution of infection and whether they can be linked to immune alterations
391 including auto-antibodies observed in patients with persistent long COVID-19 symptoms⁶⁶.

392
393

394 **Materials and Methods**

395
396

396 **Subjects and specimens**

397 Between March 2020 and April 2020, 41 patients with SARS-CoV-2 infection confirmed by
398 real-time PCR were hospitalized in the University Medical Center, Freiburg. Serum samples
399 were collected during hospitalization for routine laboratory testing. Clinical data were obtained
400 from electronic medical records. A total of 27 patients necessitating invasive mechanical
401 ventilation were included in the critical group. Fourteen patients requiring O₂ supplementation
402 were included in the severe group. Additionally, serum samples from 29 mild COVID-19 cases
403 and 30 healthy donor (HD) plasma samples were used as controls in this study.

404
405

405 **Cell culture**

406 African green monkey kidney Vero E6 cells (ATCC CRL-1586) were cultured at 37°C in
407 Dulbecco's Modified Eagle Medium (DMEM) supplemented with 10% (vol/vol) fetal calf
408 serum (FCS, Biochrom), sodium pyruvate (1x, Gibco) and 100 U/ml penicillin-Streptomycin
409 (Gibco). BW5147 mouse thymoma cells (BW, obtained from ATCC: TIB-47) were stably
410 transduced with human FcγR as previously described^{36,37}. Cells were maintained at 3x10⁵ to
411 9x10⁵ cells/ml in Roswell Park Memorial Institute medium (RPMI GlutaMAX, Gibco)
412 supplemented with 10% (vol/vol) FCS, sodium pyruvate (1x, Gibco), 100 U/ml penicillin-
413 Streptomycin (Gibco) β-mercaptoethanol (0.1 mM, Gibco). Cells were cultured at 37°C, 5%
414 CO₂. All cell lines were routinely tested for mycoplasma.

415

416 **Monitoring of antibody response to SARS-CoV-2 by ELISA**

417 Serum IgG antibody titers targeting S1- and N-SARS-CoV-2 proteins were measured using
418 commercial enzyme-linked immunosorbent assay (ELISA). Anti-S1- SARS-CoV-2 IgG was
419 measured by the anti-SARS-CoV-2 ELISA (IgG) Euroimmune Kit (Euroimmune, Lübeck,
420 Germany) according to manufacturer's protocol. Results, expressed as arbitrary units (AU),
421 were evaluated semi-quantitatively by calculation of the ratio of the extinction of the control or
422 patient sample over the extinction of the calibrator. This ratio is interpreted as follows: < 0.8
423 negative; ≥ 0.8 to <1.0 borderline; ≥ 1.1 positive. Anti-N SARS-CoV-2 IgG was detected using
424 the recomWell SARS-CoV-2 IgG Kit (Mikrogen Diagnostik GmbH, Neuried, Germany)
425 according to manufacturer's protocol. The corresponding antibody activity expressed in AU/ml
426 is calculated using the formula (absorbance of sample / absorbance of cut-off) $\times 20$. Result are
427 interpreted as follow: < 20 negative; ≥ 20 to < 24 borderline; > 24 positive. IgG against the
428 SARS-CoV-2 Spike Glycoprotein Receptor Binding Domain (RBD) were detected using
429 SARS-CoV-2 IgG ELISA Reagent Set, kindly provided by InVivo (InVivo Biotech Services
430 GmbH, Hennigsdorf, Germany) according to manufacturer's protocol.

431

432 **Fc γ R activation assay**

433 Fc γ RIIIA (CD16A, 158V) activation was measured by a cell-based assay as previously
434 described³⁸. For detection of anti-S and anti-RBD-specific Fc γ R activation we utilized SARS-
435 CoV-2-S- and RBD-coated plates (kindly provided by InVivo Biotech Services GmbH,
436 Hennigsdorf, Germany). The recombinant (S)-protein was produced under serum-free
437 conditions in mammalian cells and contains amino acid residues 1 to 1213 of the SARS-CoV-
438 2 Wuhan-Hu-1-isolate (GenBank annotation QHD43416.1). The furin cleavage site was
439 mutated, two mutations for protein stabilization were included, and the C-terminal domain was
440 replaced by a T4 trimerization sequence and a C-terminal hexa-His-Tag⁶⁷. The recombinant
441 RBD-protein represented amino acids 319 to 541 of the (S)-protein mentioned before. Both
442 recombinant proteins were purified using immobilized metal exchange chromatography
443 (IMAC) and preparative SEC under standard conditions in a regulated environment. Microtiter
444 plates were coated using 0.2 μ g recombinant (S)-protein or RBD-protein per well. N-specific
445 Fc γ R activation was determined using plates coated with SARS-CoV-2-N (Mikrogen
446 Diagnostik GmbH, Neuried, Germany). Respective plates were subsequently incubated with
447 serial dilutions of SARS-CoV-2 positive sera or control sera in RPMI supplemented with 10%
448 (vol/vol) FCS for 30 min at 37°C. All wells were thoroughly washed before co-cultivation with
449 BW5147 reporter cells for 16 h at 37°C, 5% CO₂. Cross-link activation of reporter cells was
450 performed by direct coating of target antibody to ELISA plate (Nunc Maxisorp; 96 well, flat
451 transparent), followed by a blocking step and incubation with 2×10^5 reporter cells per well.
452 For all activation assays, mouse IL-2 secretion was quantified by anti-IL-2 ELISA, as described
453 earlier. Fc γ RIIIA (CD16A) activation by multimeric sICs was measured by a recently
454 developed cell-based assay²⁵. Briefly, 2×10^5 BW5147-CD16 reporter cells were incubated with
455 SARS-CoV-2 sera in a total volume of 200 μ l for 16 h at 37°C, 5% CO₂. Incubation was
456 performed in a 96-well ELISA plate (Nunc Maxisorp) pre-treated with PBS containing 10%
457 FCS for 1 h at 4°C to avoid direct binding of serum IgG to the plate. Reporter cell mIL-2
458 secretion was quantified via ELISA as described previously³⁸.

459

460 **Purification of SARS-CoV2-S and -N specific antibodies from serum**

461 SARS-CoV-2-specific antibodies were purified using SARS-CoV-2 spike protein (S)-coated
462 plates (kindly provided by InVivo BioTech Services) and - nucleocapsid (N) - coated plates
463 recomWell SARS-CoV-2 IgG (Mikrogen Diagnostik GmbH, Neuried, Germany). Patient sera
464 were diluted 1:5 in 100 μ l (two wells per serum sample) and incubated for one hour at 37°C
465 with the S- and N-precoated plates. After washing using PBS-T (0.05% Tween 20) 100 mM

466 formic acid (30 μ l/well) was added and incubated for 5 min on an orbital shaker at room
467 temperature (RT) to elute bound IgG. Following pH neutralization using TRIS buffer (1 M),
468 the eluates were either directly processed or stored at 4°C.

469

470 **Quantitation of antigen-specific IgG amount**

471 In order to determine the relative S1- and N-SARS-CoV-2 specific IgG antibody concentration
472 of the generated eluates, S1- and N-ELISA were performed by the anti-SARS-CoV-2 ELISA
473 (IgG) Euroimmune Kit (Euroimmune, Lübeck, Germany) and anti-N SARS-CoV-2 IgG ELISA
474 (recomWell SARS-CoV-2 IgG Kit (Mikrogen Diagnostik GmbH, Neuried, Germany) as
475 aforementioned.

476

477 **Analysis of antigen-specific IgG-Fc fucosylation**

478 Fucosylation levels of S- and N-specific IgG were measured using a lectin-based ELISA assay.
479 Briefly, 96-well Maxisorb plates (Nunc®) were coated with 50 μ l/well anti-human IgG-Fab
480 fragment (MyBiosource, MBS674607) at a concentration of 2 μ g/ml, diluted in PBS for one
481 hour at 37°C. After three washing steps with PBS-T (0.05% Tween20) unspecific binding sites
482 were blocked adding 300 μ l/well Carbo-free™ blocking solution (VectorLab, Inc., SP-5040,
483 LOT: ZF0415) for one hour at room temperature. After three further washing steps, eluted
484 antibodies were serially diluted (2-fold) with PBS in a total volume of 30 μ l/well and incubated
485 for one hour at 37°C and 5% CO₂. After washing (3x) using PBS-T, 50 μ l/well of 4 μ g/ml
486 biotinylated Aleuria Aurantia lectin (AAL, lectin, VectorLab, B-1395) diluted in lectin buffer
487 (10 mM HEPES, 0.1 mM CaCl₂, 0.15 M NaCl, 0.1% Tween20) was added and incubated for
488 45 min at room temperature (RT). Following another three washing steps using PBS-T,
489 Streptavidin-Peroxidase Polymer (Sigma, S 2438), at 1 μ g/ml final concentration diluted in
490 LowCross-HRP®-buffer (Candor, Order #: 200 500) was added and incubated for one hour at
491 RT. After washing five times with PBS-T, 50 μ l/well of 1-Step™ Ultra TMB-ELISA Substrate
492 Solution (ThermoFisher, 34028) was applied and the enzyme-substrate reaction was stopped
493 after six minutes using 50 μ l/well sulphuric acid (1 M H₂SO₄). Quantification of absorbance,
494 OD_{450nm}, was performed using a Tecan M2000. Relative fucosylation for each generated pool-
495 eluate was calculated by normalizing OD_{450nm} (fucosylation) to its respective relative antigen-
496 specific IgG amount.

497

498 **PEG Precipitation**

499 Sera pools, consisting of eight different sera per pool, were diluted with varying amounts of
500 PEG8000, in order to reach a final PEG8000 concentration of 1, 2, 3.5, 5 and 7.5% respectively.
501 Mixtures were vortexed and incubated overnight at 4°C. For supernatant analysis, precipitates
502 were sedimented via centrifugation at 13.000 rpm for 30 minutes at 4°C. For Mass Spectrometry
503 analysis, PEG8000-precipitated sICs were shortly run into 10% polyacrylamide gels. After
504 over-night fixation (40% ethanol, 10% acetic acid, 50% water) and washing (3x), complete
505 lanes were excised.

506

507 **Benzonase treatment of sera**

508 Serum from six individual patients containing CD16-reactive soluble immune complexes, were
509 treated with 250 units (U) of Benzonase Nuclease (Sigma-Aldrich Chemie GmbH, Munich
510 Germany) for 1 h at 4°C. After treatment, sera were titrated in complete BW5147 culture
511 medium and tested for CD16 reactivity. Non-treated sera served as control. To verify
512 Benzonase activity in the presence of human serum, 3 μ g of pIRES-eGFP plasmid DNA
513 (Addgene) were digested with 250 U of Benzonase. Successful nucleic acid digestion was
514 visualized using a 1% agarose gel stained with Midori Green.

515

516 **Immune precipitation**

517 For mass spectrometry analysis of SARS-CoV2-S specific precipitates, individual sera
518 containing CD16-reactive soluble immune complexes were subjected to immune precipitation
519 (IP) using Pierce MS-compatible magnetic IP kit (ThermoFisher Scientific, Darmstadt,
520 Germany) according to manufacturer's protocol. Briefly 250 µl serum was incubated overnight
521 at 4°C with 5 µg of biotinylated anti-RBD-specific TRES-1-224.2.19 mouse monoclonal
522 antibody or TRES-II-480 (isotype control) (kind gift of H.M. Jäck, Erlangen) before addition
523 of streptavidin magnetic beads. Beads were subsequently collected via centrifugation and
524 elution buffer was added to detach putative precipitated antigen. The elution was dried in a
525 speed vacuum concentrator and shortly run into 10% polyacrylamide gels. After over-night
526 fixation (40% ethanol, 10% acetic acid, 50% water) and washing (3x), complete lanes were
527 excised. Antibody biotinylation was performed using a Pierce antibody biotinylation Kit for IP
528 (ThermoFisher Scientific, Darmstadt, Germany) according to manufacturer's protocol.
529

530 **Mass Spectrometry**

531 Proteins were in-gel digested with sequencing grade modified trypsin (Promega GmbH,
532 Walldorf, Germany) similar to the procedure described by Pandey et al.⁶⁸. Vacuum-dried
533 peptides were dissolved in 0.5% trifluoroacetic acid, loaded onto a trap column (C18
534 PepMap100, 5 µm particles, Thermo Fisher Scientific GmbH, Dreieich, Germany) with 0.05%
535 trifluoroacetic acid (4 min, 10 µL/min) and separated on a C18 reversed phase column
536 (SilicaTip™ emitter, 75 µm i.d., 8 µm tip, New Objective, Inc, Littleton, USA, manually packed
537 23 cm with ReproSil-Pur ODS-3, 3 µm particles, Dr. A. Maisch HPLC GmbH, Ammerbuch-
538 Entringen, Germany; flow rate: 300 nL/min). For sample injection and multi-step gradient
539 formation (eluent "A": 0.5% acetic acid in water; eluent "B": 0.5% acetic acid in 80%
540 acetonitrile / 20% water; gradient length / acquisition time: 100 min or 175 min) an UltiMate
541 3000 RSLCnano system (Thermo Fisher Scientific GmbH, Dreieich, Germany) was used.
542 Eluting peptides were electrosprayed at 2.3 kV via a Nanospray Flex ion source into a Q
543 Exactive HF-X hybrid quadrupole-orbitrap mass spectrometer (both Thermo Fisher Scientific
544 GmbH, Dreieich, Germany) and analyzed by data-dependent acquisition with HCD (higher
545 energy collisional dissociation) fragmentation of doubly, triply and quadruply charged ions
546 (loop count and dynamic exclusion dependent on the gradient length). Peak lists were generated
547 with ProteoWizard msConvert (<http://proteowizard.sourceforge.net/>; version 3.0.11098), linear
548 shift mass recalibrated (after a preliminary database search) using software developed in-house
549 and searched against a database containing the SARS-CoV-2 UniProtKB reference proteome
550 (proteome ID: UP000464024), all human UniProtKB/Swiss-Prot entries, and optionally (to
551 reduce the number of incorrectly assigned matches) selected bacterial proteins (finally the
552 *Pseudomonas fluorescens* (strain SBW25) reference proteome; proteome ID: UP000002332)
553 with Mascot 2.6.2 (Matrix Science Ltd, London, UK; peptide mass tolerance: ± 5 ppm;
554 fragment mass tolerance: ± 20 mmu; one missed trypsin cleavage and common variable
555 modifications allowed).
556

557 **Neutralization assay**

558 Serum neutralization capacity was analyzed as previously described⁶⁹. Briefly, VeroE6 cells
559 were seeded in 12-well plates at a density of 2.8×10^5 cells/well 24 h prior to infection. Serum
560 samples were diluted at ratios of 1:16, 1:32 and 1:64 in 50 µL PBS total volume. Negative
561 controls (PBS without serum) were included for each serum. Diluted sera and negative controls
562 were subsequently mixed with 90 plaque forming units (PFU) of authentic SARS-CoV-2 (B.1)
563 in 50 µl PBS (1600 PFU/mL) resulting in final sera dilution ratios of 1:32, 1:64, and 1:128.
564 Following incubation at RT for 1 h, 400 µL PBS was added to each sample and the mixture
565 was subsequently used to infect VeroE6 cells. After 1.5 h of incubation at RT, inoculum was
566 removed and the cells were overlaid with 0.6% Oxoid-agar in DMEM, 20 mM HEPES (pH
567 7.4), 0.1% NaHCO₃, 1% BSA and 0.01% DEAE-Dextran. Cells were fixed 48h post-infection

568 (4% formaldehyde for 30 minutes). Upon removal of the agar overlay, plaque neutralization
569 was visualized using 1% crystal violet. PFU were counted manually. Plaques counted for
570 serum-treated wells were compared to the average number of plaques in the untreated negative
571 controls, which were set to 100%.

572

573 **Ethics**

574 The protocol of this study conforms to the ethical guidelines of the 1975 Declaration of Helsinki
575 and was approved by the institutional ethical committee of the University of Freiburg (EK
576 153/20). Written informed consent was obtained from participants and the study was conducted
577 according to federal guidelines, local ethics committee regulations (Albert-Ludwigs-
578 Universität, Freiburg, Germany: No. F-2020-09-03-160428 and no. 322/20)

579

580 **Author contribution**

581 Conceived and designed the experiments: J.A., A.M-P., S.G., P.K., A.L, V.F., M.S., H.H.

582 Performed the experiments: J.A., N.G., U.S., S.G., K. C., W.B.

583 Analyzed the data: J.A., S.G., P.K., V.F., K.C., A.M-P., W.B., C.K.

584 Contributed/reagent/sample material: A.B.G., D.H., T.W., N.G.M.

585 Writing and original draft preparation: J.A., S.G., P.K., V.F.

586 Review and editing: H.H., M.S., K.C.

587 Conceptualization: V.F., H.H.

588

589 **Acknowledgements**

590 We thank Sophia Ruben and Torsten Schulz from InVivo Bio Tech Services for preparing
591 SARS-CoV-2 (S)- and RBD- coated plates and preparing the SARS-CoV-2 IgG ELISA
592 Reagent Set. We thank Hans-Martin Jäck for providing TRES-1-224.2.19 and TRES-II-480
593 monoclonal antibodies and Quinnlan David for critically reading the manuscript. We also thank
594 Andreas Schlosser for validation of our Mass Spectrometry data. This work was supported by
595 the Bundesministerium fuer Bildung und Forschung (BMBF) through the Deutsches Zentrum
596 fuer Luft- und Raumfahrt, Germany, (DLR, grant number 01KI2077) and by the Federal State
597 of Baden-Wuerttemberg, Germany, MWK-Sonderfoerdermaßnahme COVID-19/AZ.:33-
598 7533.-6-21/7/2 to MS. This work was also supported by an intramural junior investigator fund
599 of the Faculty of Medicine to PK (EQUIP - Funding for Medical Scientists, Faculty of
600 Medicine, University of Freiburg) and “NaFoUniMedCovid19“ (FKZ: 01KX2021 - COVIM to
601 H.H., FKZ 100493916 B-FAST to H.H.) and DFG HE2526/9-1 to H.H.. A. Lothar is a member
602 of SFB1425, funded by the Deutsche Forschungsgemeinschaft (DFG, German Research
603 Foundation #422681845). The funders had no role in the study design, data analysis, data
604 interpretation, and in the writing of this report. All authors had full access to the data in the
605 study and accept responsibility to submit for publication.

606

607 **Statistical analyses**

608 Statistical analyses were performed using linear statistical models. i.e. the two-group
609 comparisons were made based on the t-statistic of the estimated effects. Differences over more
610 than two groups were tested by Analysis of Variance (ANOVA) and multiple testing for
611 subsequent two-group comparisons was then considered by performing Games-Howell post-
612 hoc tests. For the time course data, patient differences were treated as random effects in a linear
613 mixed effects model with time and clinical course (severe vs. critical) as fixed main and
614 interaction effects. All analyses were performed at the log₂ scale. Assumptions about variance
615 heterogeneity and normal distribution were checked by visual inspection of diagnostic plots.

616

617 **Data and materials availability**

618 All data associated with this study are present in the paper or Supplementary Materials.

619 **References**

- 620
- 621 1. Zhu N, Zhang D, Wang W, et al. A Novel Coronavirus from Patients with Pneumonia in China,
622 2019. *N Engl J Med.* 2020;382(8):727-733.
- 623 2. Dong E, Du H, Gardner L. An interactive web-based dashboard to track COVID-19 in real time.
624 *Lancet Infect Dis.* 2020;20(5):533-534.
- 625 3. Chen G, Wu D, Guo W, et al. Clinical and immunological features of severe and moderate
626 coronavirus disease 2019. *J Clin Invest.* 2020;130(5):2620-2629.
- 627 4. Petrilli CM, Jones SA, Yang J, et al. Factors associated with hospital admission and critical illness
628 among 5279 people with coronavirus disease 2019 in New York City: prospective cohort study.
629 *BMJ.* 2020;369:m1966.
- 630 5. Huang C, Wang Y, Li X, et al. Clinical features of patients infected with 2019 novel coronavirus
631 in Wuhan, China. *Lancet.* 2020;395(10223):497-506.
- 632 6. Wang F, Hou H, Luo Y, et al. The laboratory tests and host immunity of COVID-19 patients with
633 different severity of illness. *JCI Insight.* 2020;5(10).
- 634 7. Felsenstein S, Herbert JA, McNamara PS, Hedrich CM. COVID-19: Immunology and treatment
635 options. *Clin Immunol.* 2020;215:108448.
- 636 8. Wu C, Chen X, Cai Y, et al. Risk Factors Associated With Acute Respiratory Distress Syndrome
637 and Death in Patients With Coronavirus Disease 2019 Pneumonia in Wuhan, China. *JAMA*
638 *Intern Med.* 2020;180(7):934-943.
- 639 9. Magleby R, Westblade LF, Trzebucki A, et al. Impact of SARS-CoV-2 Viral Load on Risk of
640 Intubation and Mortality Among Hospitalized Patients with Coronavirus Disease 2019. *Clin*
641 *Infect Dis.* 2020.
- 642 10. Ruan Q, Yang K, Wang W, Jiang L, Song J. Correction to: Clinical predictors of mortality due to
643 COVID-19 based on an analysis of data of 150 patients from Wuhan, China. *Intensive Care Med.*
644 2020;46(6):1294-1297.
- 645 11. Zhou F, Yu T, Du R, et al. Clinical course and risk factors for mortality of adult inpatients with
646 COVID-19 in Wuhan, China: a retrospective cohort study. *Lancet.* 2020;395(10229):1054-1062.
- 647 12. Yang X, Yu Y, Xu J, et al. Clinical course and outcomes of critically ill patients with SARS-CoV-2
648 pneumonia in Wuhan, China: a single-centered, retrospective, observational study. *Lancet*
649 *Respir Med.* 2020;8(5):475-481.
- 650 13. Richardson S, Hirsch JS, Narasimhan M, et al. Presenting Characteristics, Comorbidities, and
651 Outcomes Among 5700 Patients Hospitalized With COVID-19 in the New York City Area. *JAMA.*
652 2020;323(20):2052-2059.
- 653 14. Zhou Y, Fu B, Zheng X, et al. Pathogenic T-cells and inflammatory monocytes incite
654 inflammatory storms in severe COVID-19 patients. *National Science Review.* 2020;7(6):998-
655 1002.
- 656 15. Long QX, Liu BZ, Deng HJ, et al. Antibody responses to SARS-CoV-2 in patients with COVID-19.
657 *Nat Med.* 2020;26(6):845-848.
- 658 16. Diao B, Wang C, Tan Y, et al. Reduction and Functional Exhaustion of T Cells in Patients With
659 Coronavirus Disease 2019 (COVID-19). *Front Immunol.* 2020;11:827.
- 660 17. Zhang JM, An J. Cytokines, inflammation, and pain. *Int Anesthesiol Clin.* 2007;45(2):27-37.
- 661 18. Vogelpoel LT, Baeten DL, de Jong EC, den Dunnen J. Control of cytokine production by human
662 fc gamma receptors: implications for pathogen defense and autoimmunity. *Front Immunol.*
663 2015;6:79.
- 664 19. Ritz J, Schmidt RE, Michon J, Hercend T, Schlossman SF. Characterization of functional surface
665 structures on human natural killer cells. *Adv Immunol.* 1988;42:181-211.
- 666 20. Werfel T, Uciechowski P, Tetteroo PA, Kurrle R, Deicher H, Schmidt RE. Activation of cloned
667 human natural killer cells via Fc gamma RIII. *J Immunol.* 1989;142(4):1102-1106.
- 668 21. Bruhns P, Jonsson F. Mouse and human FcR effector functions. *Immunol Rev.* 2015;268(1):25-
669 51.

- 670 22. Zubler RH, Nydegger U, Perrin LH, et al. Circulating and intra-articular immune complexes in
671 patients with rheumatoid arthritis. Correlation of 125I-Clq binding activity with clinical and
672 biological features of the disease. *J Clin Invest.* 1976;57(5):1308-1319.
- 673 23. Levinsky RJ. Role of circulating soluble immune complexes in disease. *Arch Dis Child.*
674 1978;53(2):96-99.
- 675 24. Levinsky RJ, Cameron JS, Soothill JF. Serum immune complexes and disease activity in lupus
676 nephritis. *Lancet.* 1977;1(8011):564-567.
- 677 25. Chen H, Maul-Pavicic A, Holzer M, et al. FcγR responses to soluble immune complexes are
678 governed by solubility and size. *bioRxiv.* 2021:2020.2011.2011.378232.
- 679 26. Wang TT, Ravetch JV. Immune complexes: not just an innocent bystander in chronic viral
680 infection. *Immunity.* 2015;42(2):213-215.
- 681 27. Carreno LJ, Pacheco R, Gutierrez MA, Jacobelli S, Kalergis AM. Disease activity in systemic lupus
682 erythematosus is associated with an altered expression of low-affinity Fc gamma receptors
683 and costimulatory molecules on dendritic cells. *Immunology.* 2009;128(3):334-341.
- 684 28. Faik I, van Tong H, Lell B, Meyer CG, Kremsner PG, Velavan TP. Pyruvate Kinase and Fcγ
685 Receptor Gene Copy Numbers Associated With Malaria Phenotypes. *J Infect Dis.*
686 2017;216(2):276-282.
- 687 29. Xu Z, Shi L, Wang Y, et al. Pathological findings of COVID-19 associated with acute respiratory
688 distress syndrome. *Lancet Respir Med.* 2020;8(4):420-422.
- 689 30. Channappanavar R, Perlman S. Pathogenic human coronavirus infections: causes and
690 consequences of cytokine storm and immunopathology. *Seminars in Immunopathology.*
691 2017;39(5):529-539.
- 692 31. Smits SL, de Lang A, van den Brand JM, et al. Exacerbated innate host response to SARS-CoV
693 in aged non-human primates. *PLoS Pathog.* 2010;6(2):e1000756.
- 694 32. Rockx B, Baas T, Zornetzer GA, et al. Early upregulation of acute respiratory distress syndrome-
695 associated cytokines promotes lethal disease in an aged-mouse model of severe acute
696 respiratory syndrome coronavirus infection. *J Virol.* 2009;83(14):7062-7074.
- 697 33. Hoepel W, Chen HJ, Geyer CE, et al. High titers and low fucosylation of early human anti-SARS-
698 CoV-2 IgG promote inflammation by alveolar macrophages. *Sci Transl Med.* 2021;13(596).
- 699 34. Zohar T, Alter G. Dissecting antibody-mediated protection against SARS-CoV-2. *Nat Rev*
700 *Immunol.* 2020;20(7):392-394.
- 701 35. Lu LL, Suscovich TJ, Fortune SM, Alter G. Beyond binding: antibody effector functions in
702 infectious diseases. *Nat Rev Immunol.* 2018;18(1):46-61.
- 703 36. Kolb P, Hoffmann K, Sievert A, et al. Human Cytomegalovirus antagonizes activation of
704 Fcγ receptors by distinct and synergizing modes of IgG manipulation. *Elife.* 2021;10.
- 705 37. Kolb P, Sijmons S, McArdle MR, et al. Identification and Functional Characterization of a Novel
706 Fc Gamma-Binding Glycoprotein in Rhesus Cytomegalovirus. *J Virol.* 2019;93(4).
- 707 38. Corrales-Aguilar E, Trilling M, Reinhard H, et al. A novel assay for detecting virus-specific
708 antibodies triggering activation of Fc gamma receptors. *J Immunol Methods.* 2013;387(1-
709 2):21-35.
- 710 39. Perez-Portilla A, Moraru M, Blazquez-Moreno A, et al. Identification of the first cases of
711 complete CD16A deficiency: Association with persistent EBV infection. *J Allergy Clin Immunol.*
712 2020;145(4):1288-1292.
- 713 40. Corrales-Aguilar E, Trilling M, Reinhard H, et al. Highly individual patterns of virus-immune IgG
714 effector responses in humans. *Medical microbiology and immunology.* 2016;205(5):409-424.
- 715 41. Chakraborty S, Gonzalez J, Edwards K, et al. Proinflammatory IgG Fc structures in patients with
716 severe COVID-19. *Nat Immunol.* 2021;22(1):67-73.
- 717 42. High titers and low fucosylation of early human anti-SARS-CoV-2 IgG promote inflammation by
718 alveolar macrophages. *Sci Transl Med.* 2021.
- 719 43. Larsen MD, de Graaf EL, Sonneveld ME, et al. Afucosylated IgG characterizes enveloped viral
720 responses and correlates with COVID-19 severity. *Science.* 2021;371(6532).

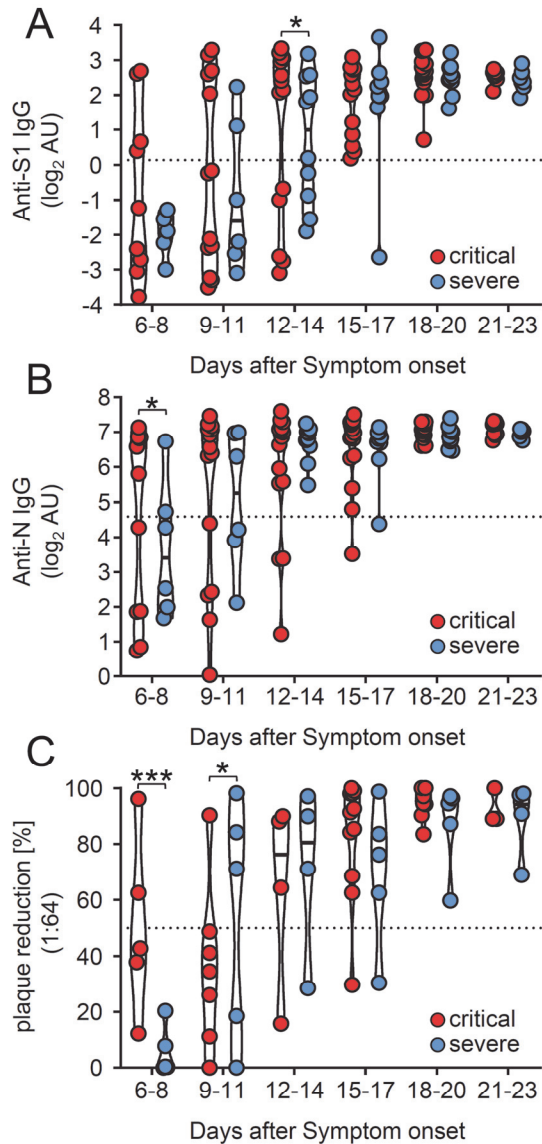
- 721 44. Li T, DiLillo DJ, Bournazos S, Giddens JP, Ravetch JV, Wang LX. Modulating IgG effector function
722 by Fc glycan engineering. *Proceedings of the National Academy of Sciences of the United States*
723 *of America*. 2017;114(13):3485-3490.
- 724 45. Roncati L, Ligabue G, Fabbiani L, et al. Type 3 hypersensitivity in COVID-19 vasculitis. *Clinical*
725 *Immunology*. 2020;217.
- 726 46. Roe K. High COVID-19 virus replication rates, the creation of antigen-antibody immune
727 complexes and indirect haemagglutination resulting in thrombosis. *Transbound Emerg Dis*.
728 2020;67(4):1418-1421.
- 729 47. Zhang Y, Xiao M, Zhang S, et al. Coagulopathy and Antiphospholipid Antibodies in Patients with
730 Covid-19. *N Engl J Med*. 2020;382(17):e38.
- 731 48. Creighton WD, Lambert PH, Miescher PA. Detection of antibodies and soluble antigen-
732 antibody complexes by precipitation with polyethylene glycol. *J Immunol*. 1973;111(4):1219-
733 1227.
- 734 49. Veras FP, Pontelli MC, Silva CM, et al. SARS-CoV-2-triggered neutrophil extracellular traps
735 mediate COVID-19 pathology. *J Exp Med*. 2020;217(12).
- 736 50. Zuo Y, Yalavarthi S, Shi H, et al. Neutrophil extracellular traps in COVID-19. *JCI Insight*.
737 2020;5(11).
- 738 51. Bonaventura A, Vecchie A, Dagna L, et al. Endothelial dysfunction and immunothrombosis as
739 key pathogenic mechanisms in COVID-19. *Nat Rev Immunol*. 2021;21(5):319-329.
- 740 52. Horwitz JA, Bar-On Y, Lu CL, et al. Non-neutralizing Antibodies Alter the Course of HIV-1
741 Infection In Vivo. *Cell*. 2017;170(4):637-648 e610.
- 742 53. Forthal DN, Moog C. Fc receptor-mediated antiviral antibodies. *Curr Opin HIV AIDS*.
743 2009;4(5):388-393.
- 744 54. DiLillo DJ, Tan GS, Palese P, Ravetch JV. Broadly neutralizing hemagglutinin stalk-specific
745 antibodies require FcγR interactions for protection against influenza virus in vivo. *Nat*
746 *Med*. 2014;20(2):143-151.
- 747 55. Hessel AJ, Hangartner L, Hunter M, et al. Fc receptor but not complement binding is important
748 in antibody protection against HIV. *Nature*. 2007;449(7158):101-104.
- 749 56. Li K, Huang B, Wu M, et al. Dynamic changes in anti-SARS-CoV-2 antibodies during SARS-CoV-
750 2 infection and recovery from COVID-19. *Nature communications*. 2020;11(1):6044.
- 751 57. Thanadetsunorn C, Ngamjanyaporn P, Setthaudom C, Hodge K, Saengpiya N, Pisitkun P. The
752 model of circulating immune complexes and interleukin-6 improves the prediction of disease
753 activity in systemic lupus erythematosus. *Sci Rep*. 2018;8(1):2620.
- 754 58. Woodruff MC, Ramonell RP, Nguyen DC, et al. Extrafollicular B cell responses correlate with
755 neutralizing antibodies and morbidity in COVID-19. *Nat Immunol*. 2020;21(12):1506-1516.
- 756 59. Wang EY, Mao T, Klein J, et al. Diverse functional autoantibodies in patients with COVID-19.
757 *Nature*. 2021.
- 758 60. Zuo Y, Estes SK, Ali RA, et al. Prothrombotic autoantibodies in serum from patients hospitalized
759 with COVID-19. *Sci Transl Med*. 2020;12(570).
- 760 61. Chang SE, Feng A, Meng W, et al. New-Onset IgG Autoantibodies in Hospitalized Patients with
761 COVID-19. *medRxiv*. 2021.
- 762 62. Bastard P, Rosen LB, Zhang Q, et al. Autoantibodies against type I IFNs in patients with life-
763 threatening COVID-19. *Science*. 2020;370(6515).
- 764 63. Heidelberger M, Kendall FE. A Quantitative Study of the Precipitin Reaction between Type Iii
765 Pneumococcus Polysaccharide and Purified Homologous Antibody. *J Exp Med*. 1929;50(6):809-
766 823.
- 767 64. Gharebaghi N, Nejadrahim R, Mousavi SJ, Sadat-Ebrahimi SR, Hajizadeh R. The use of
768 intravenous immunoglobulin gamma for the treatment of severe coronavirus disease 2019: a
769 randomized placebo-controlled double-blind clinical trial. *BMC Infect Dis*. 2020;20(1):786.
- 770 65. Shock A, Humphreys D, Nimmerjahn F. Dissecting the mechanism of action of intravenous
771 immunoglobulin in human autoimmune disease: Lessons from therapeutic modalities
772 targeting Fcγ receptors. *J Allergy Clin Immunol*. 2020;146(3):492-500.

- 773 66. Wallukat G, Hohberger B, Wenzel K, et al. Functional autoantibodies against G-protein coupled
774 receptors in patients with persistent Long-COVID-19 symptoms. *J Transl Autoimmun.*
775 2021;4:100100.
- 776 67. Amanat F, Stadlbauer D, Strohmeier S, et al. A serological assay to detect SARS-CoV-2
777 seroconversion in humans. *Nat Med.* 2020;26(7):1033-1036.
- 778 68. Pandey A, Andersen JS, Mann M. Use of mass spectrometry to study signaling pathways. *Sci*
779 *STKE.* 2000;2000(37):pl1.
- 780 69. Tönshoff B, Müller B, Elling R, et al. Prevalence of SARS-CoV-2 Infection in Children and Their
781 Parents in Southwest Germany. *JAMA Pediatrics.* 2021;175(6):586-593.
- 782
- 783
- 784
- 785
- 786

787 **Figure 1**

788

789



790

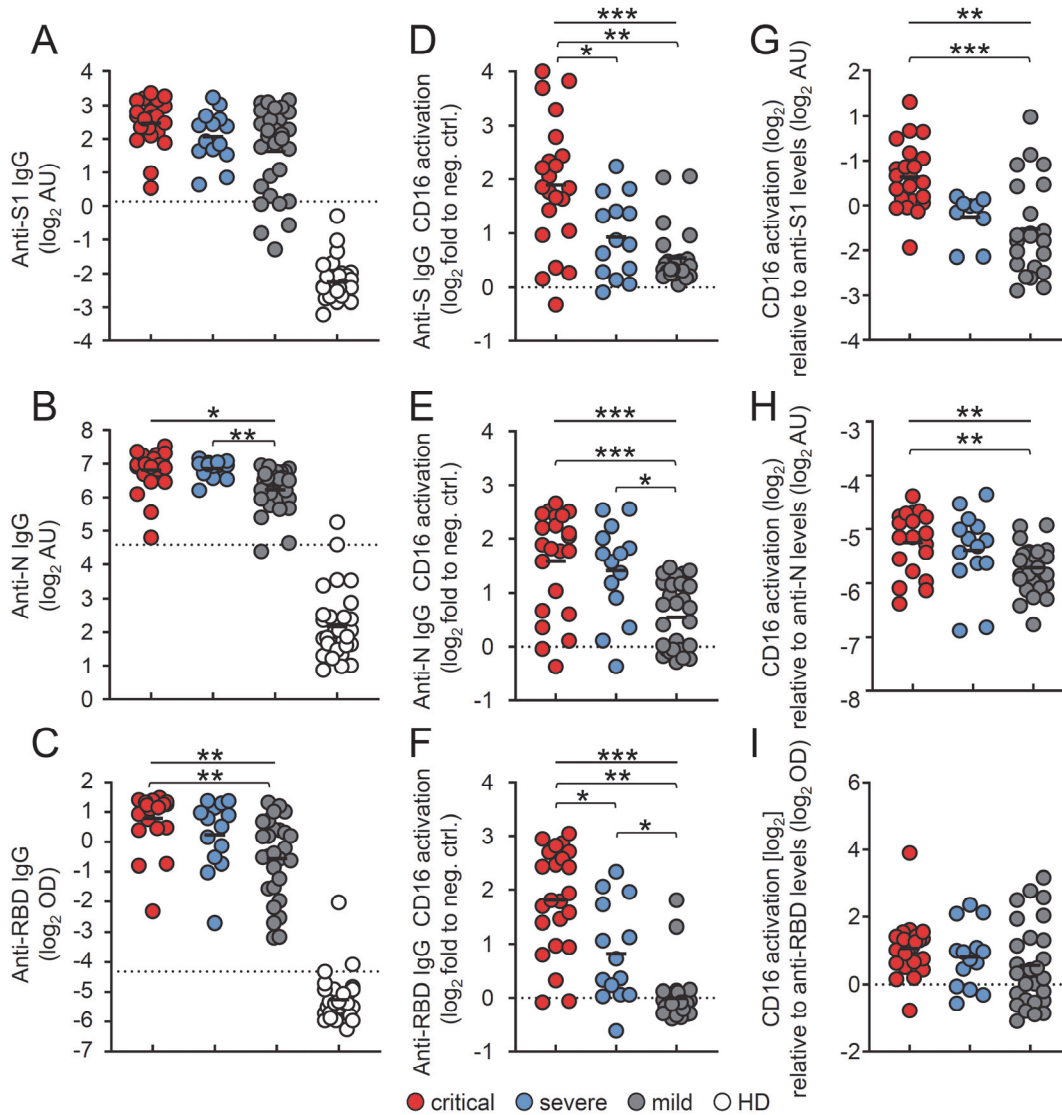
791 **IgG responses against different SARS-CoV-2 proteins across severe and critical clinical**

792 **course of disease.**

793 IgG antibody levels were analyzed in longitudinal serum samples from hospitalized SARS-
794 CoV-2 infected individuals. 27 patients were categorized as critically diseased when in need of
795 invasive mechanical ventilation (red symbols) compared to 14 severely diseased patients who
796 did not require invasive ventilation (blue symbols). (A) IgG response against SARS-CoV-2 S1
797 -protein and (B) SARS-CoV-2 N-protein as determined by commercial ELISA assays. Dotted
798 lines represent cut-off values for commercial S1- and N- specific ELISA assays. Each dot
799 represents the mean value obtained by the analysis of all samples which were available at the
800 indicated time points following symptom onset. Solid black lines indicate the median. (C)
801 Serum neutralization capacity against SARS-CoV-2 measured by a plaque reduction assay. Sera
802 were considered neutralizing upon 50% plaque reduction (dotted line) at a 1:64 dilution. Solid
803 black lines indicate the median. Significant differences were tested using a linear mixed effects
804 model (***, $p < 0.001$; *, $p < 0.05$).

805

806 **Figure 2**
 807
 808

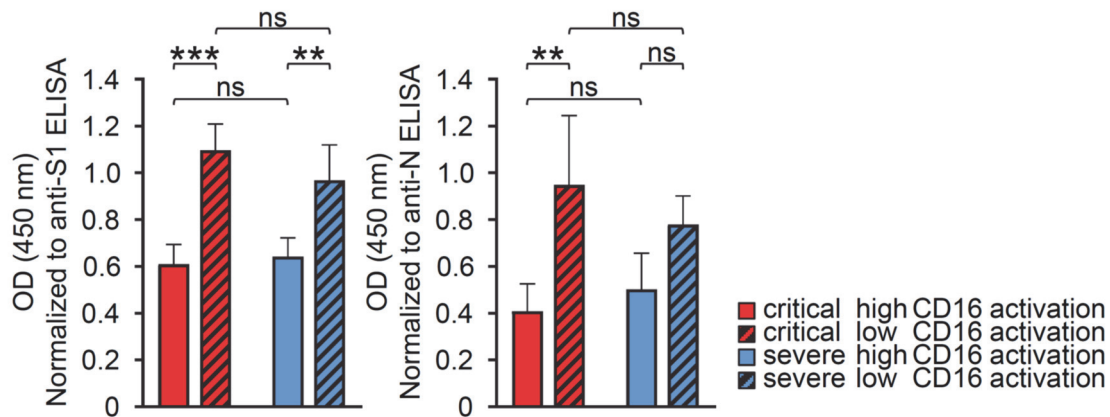


809
 810 **CD16 activation by SARS-CoV-2 - specific IgG is enhanced in critically diseased patients.**
 811 Fc γ RIII activation by SARS-CoV-2-specific IgG on BW5147 reporter cells in serum samples
 812 obtained 13-25 days following symptom onset from 23 critically (red symbols) and 14 severely
 813 (blue symbols) diseased patients. Between 2 to 8 samples/patient were analyzed depending on
 814 the availability of sample material. Sera from 29 non-hospitalized patients with mild SARS-
 815 CoV-2 infection (grey symbols) and 30 healthy donors (open circles) served as reference. Each
 816 symbol represents the mean value of all available samples per patient. (A, B, C) ELISA levels
 817 for S1- N- and RBD-specific IgG. Dotted lines represent cut-off values for commercial S1-, N-
 818 and RBD - specific ELISA assays. Solid black lines indicate the mean. (D, E, F) Fc γ RIII
 819 activation by S-, N- and RBD-specific IgG expressed as \log_2 fold change relative to negative
 820 control. Solid black lines indicate the mean. (G, H, I) Fc γ RIII activation, expressed as \log_2
 821 values relative to SARS-CoV-2-specific IgG titers. Solid black lines indicate the mean.
 822 Significant differences over all three groups were tested by ANOVA and pairwise group
 823 comparison was made by Games-Howell post-hoc tests (***, $p < 0.001$; **, $p < 0.01$; *, $p < 0.05$).
 824

825 **Figure 3**

826

827



828

829

Anti SARS-CoV-2 IgG Fc core fucosylation in critical and severe COVID-19 cases.

830

831

832

833

834

835

836

837

838

839

IgG-Fc core fucosylation levels of SARS-CoV-2 -specific IgG in critically (red bars) and severely (blue bars) diseased COVID-19 patients. Analysis was carried out on a pool of 5 different sera. Measured OD values for fucosylation of the generated eluates were normalized to their respective IgG titers determined by antigen-specific S1 and N ELISA. A) S-IgG-Fc-fucosylation and B) N-IgG-Fc-fucosylation in critically and severely diseased patients characterized by either high (red) or low (patterned) CD16-activation levels in the FcγR activation reporter assay. The mean and standard deviation (SD) of at least three independent experiments is depicted. Statistical tests using a two-factorial linear model indicate three significant differences between the low and high categories (***, $p < 0.001$; **, $p < 0.01$; *, $p < 0.05$; ns = not significant).

840

841

842

843

844

845

846

847

848

849

850

851

852

853

854

855

856

857

858

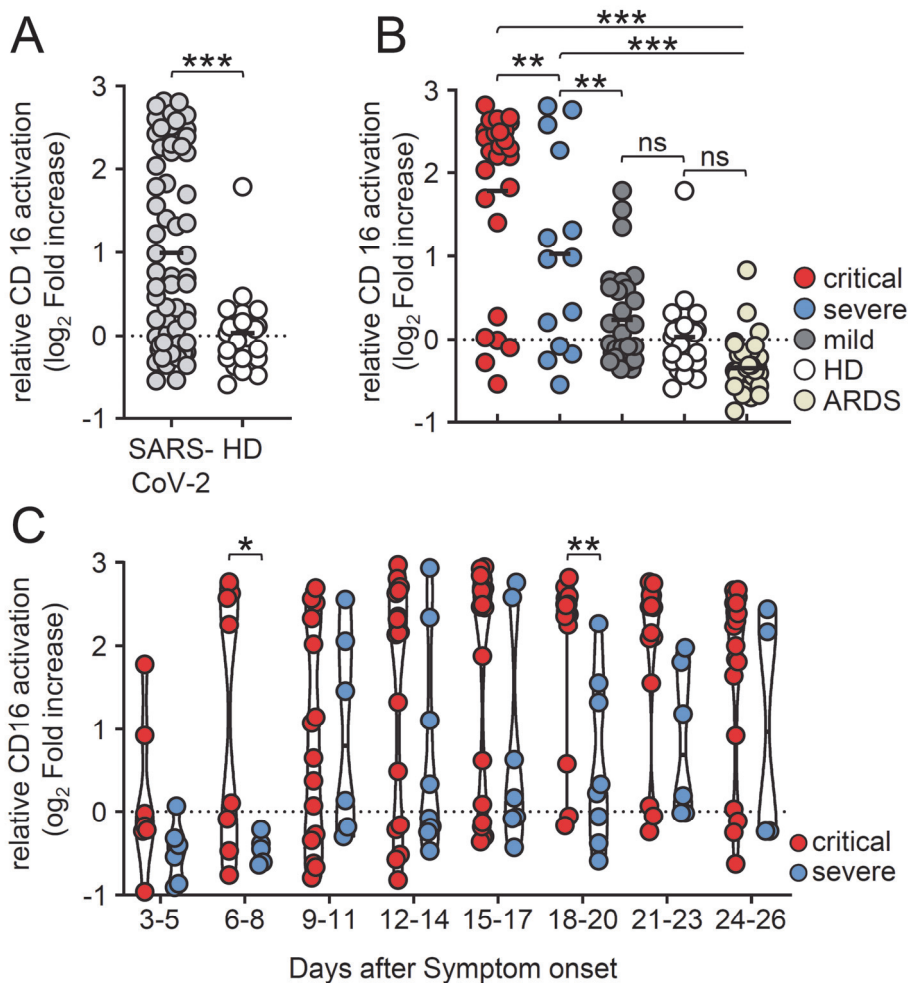
859

860

861

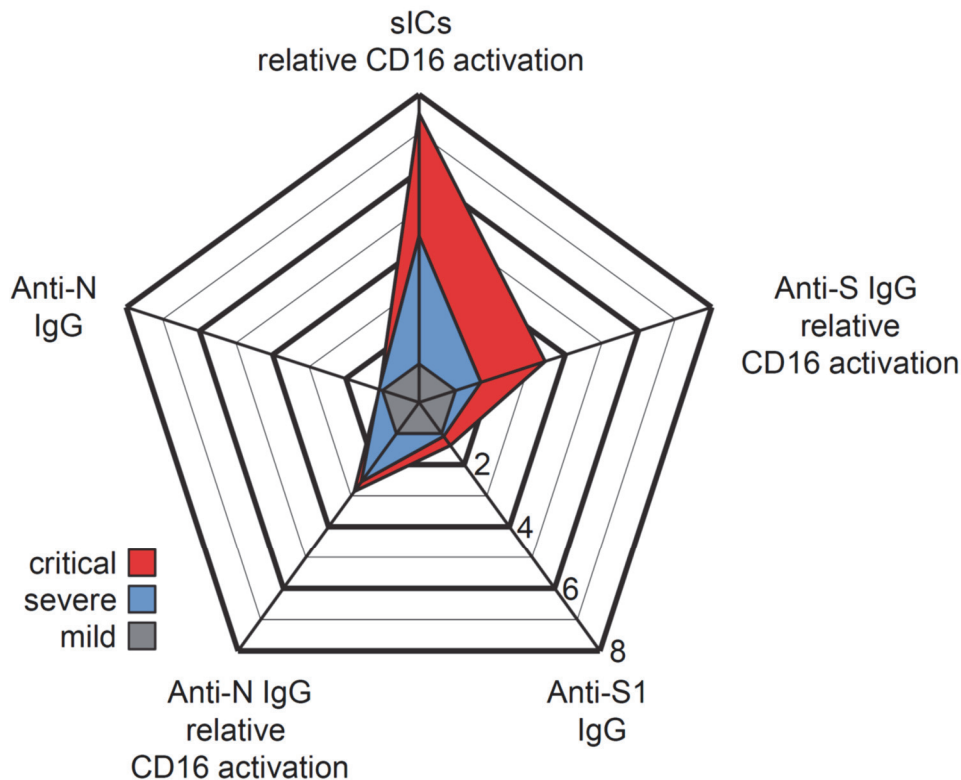
862

863 **Figure 4**
 864
 865



866
 867 **Severe COVID-19 disease coincides with high CD16 activation by sICs.**
 868 Serial serum samples obtained 13-25 days after onset of symptoms were analyzed in a cell-
 869 based reporter assay which is sensitive to sIC amount and size²⁵. FcγR activation is shown as
 870 log₂ fold change relative to negative control. Each symbol represents the mean value obtained
 871 by the analysis of all samples available in the indicated time range for each individual patient.
 872 A) Analysis of CD16 activation by sICs in SARS-CoV-2-infected patients compared to healthy
 873 blood donors B) Levels of IC-mediated CD16 activation across severe, critical and mild clinical
 874 courses of COVID-19 disease, in healthy donors (HD) and in non-COVID-19 patients who
 875 developed acute respiratory distress syndrome (ARDS). Solid black lines indicate the mean.
 876 Two-group comparisons with the linear model indicate significant differences between critical
 877 cases and all other groups, as well as between severe cases and all other groups (***, p<0.001;
 878 **, p<0.01). No significant differences (p>0.05) have been found for the comparisons mild vs.
 879 healthy and for HD vs. ARDS. C) Kinetics of IC-mediated CD16 activation in critically and
 880 severely diseased patients. Solid black lines indicate the median. The mixed effects model
 881 indicates two time points with significant differences (**, p<0.01; *, p<0.05).
 882
 883

884 **Figure 5**
885
886



887
888 **Summary of antibody features from SARS-CoV-2-infected patients with critical and**
889 **severe disease.**

890 Relative multivariate antibody features illustrated as radar chart in critically (red) or severely
891 (blue) diseased COVID-19 patients normalized to the corresponding features of patients with
892 mild infection (grey). Each spoke represents one of the following variables: ELISA (S1-IgG,
893 N-IgG,) and CD16 activation (S-IgG, N-IgG, multimeric sICs). Arithmetic mean values of \log_2
894 values were calculated for each group (days 13-25 post symptom onset) respectively. The fold
895 change compared to mildly diseased patients is shown.

896
897
898
899
900
901
902
903
904
905
906
907
908
909
910
911
912

913 **Table 1: Clinical characteristics of the hospitalized SARS-CoV-2 patients.**
 914 Patients were categorized as either severely (hospitalized, requiring O₂ supplementation, n=14)
 915 or critically diseased (hospitalized and in need of invasive mechanical ventilation, n=27).
 916 Diagnostic markers are depicted as mean and SD (in brackets) of all analyzed laboratory
 917 parameters obtained 13-25 days post symptom onset. Percentage [%] is indicated.
 918
 919

	All patients n: 41	%	critical n: 27	%	severe n: 14	%
Age [years]	Ø 68 (31-90)	-	Ø 63 (39-79)	-	Ø 76 (31-90)	-
Female	8	19.5	5	18.5	3	21.4
Male	33	80.5	22	81.5	11	78.6
Comorbidities						
Hypertension	21	51.2	12	44.4	9	64.3
Cardiovascular disease	14	34.1	5	18.5	9	64.3
Pulmonary disease	6	14.6	2	7.4	4	28.6
Chronic kidney disease	6	14.6	1	3.7	5	35.7
Diabetes	10	24.4	6	22.2	4	28.6
Malignancy	8	19.5	4	14.8	4	28.6
none	6	14.6	6	22.2	0	0
Diagnostic markers						
Interleukin-6 [pg/ml] Ø	1012.8	-	1452.1 (3774.6)	-	46.1 (26.8)	-
Procalcitonin [ng/ml] Ø	7	-	9.9 (21.9)	-	0.17 (0.11)	-
C- reactive protein [mg/l] Ø	128.1	-	162.2 (75.8)	-	65.3 (47.1)	-
Complications						
Bacterial superinfection	16	39	11	40.7	5	35.7
Treatment						
Hydroxychloroquine, Ritonavir+ Lopinavir (Kaletra®)	24	58.5	18	66.7	6	42.9
Fatal outcome						
Total	11	26.8	10	37	1	7.1

920

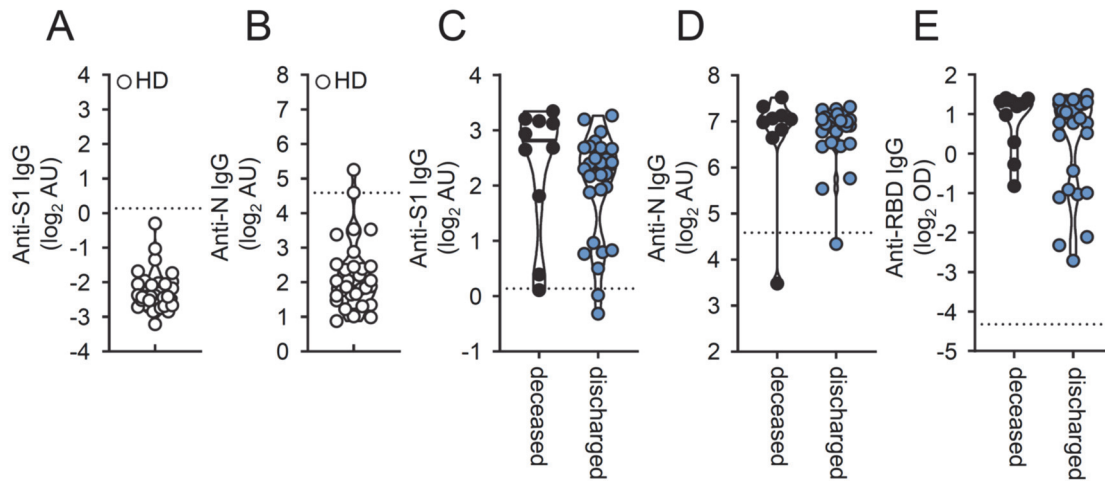
921 **Supplementary Figures**

922

923

924 **Figure 1-figure supplement 1.**

925



926

927

928 **SARS-CoV-2 specific IgG levels in seronegative patients and according to disease**

929 **outcome.**

930 A) S1- and B) N-specific IgG levels in 30 healthy donors. Solid black lines indicate the median.

931 C) Cumulative S1-, D) N- and E) RBD-specific IgG levels measured 13-25 days after symptom

932 onset in deceased (black symbols) and not deceased COVID-19 patients (blue symbols). Each

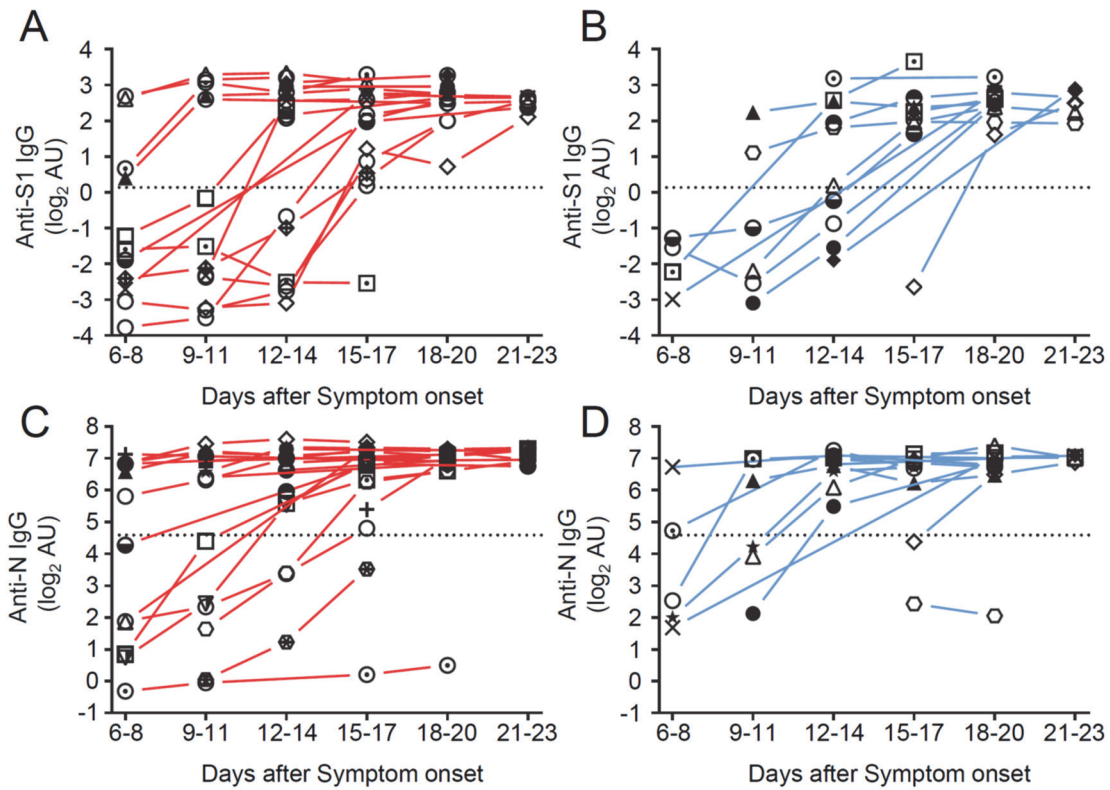
933 symbol represents the mean value obtained by the analysis of all samples available in the

934 indicated time range for each individual patient. Solid black lines indicate the median.

935

936

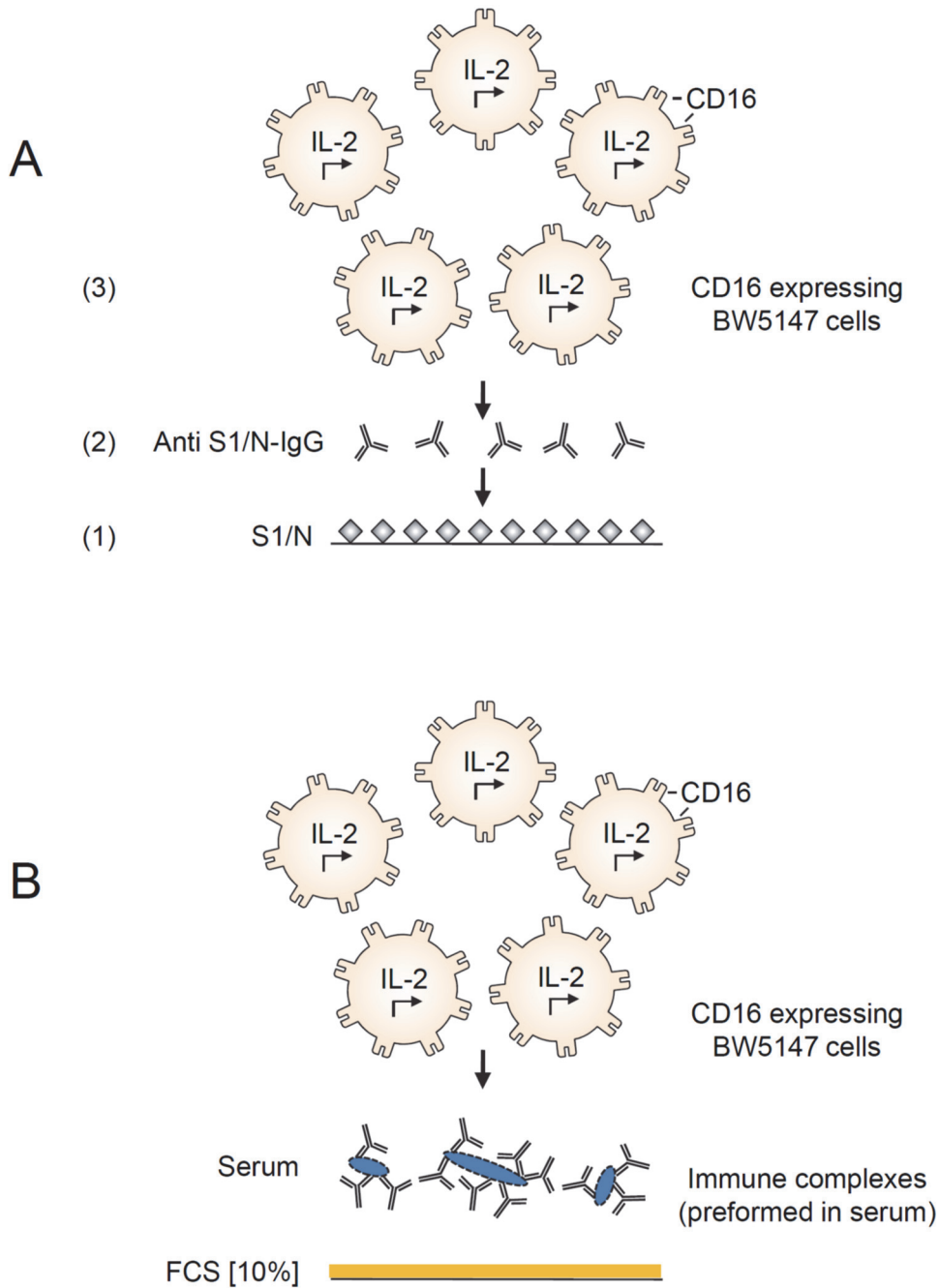
937 **Figure 1-figure supplement 2.**
938



939 **Longitudinal changes in anti- SARS-CoV-2 IgG titers in severely and critically diseased**
940 **patients.**
941

942 Serial serum samples were collected from hospitalized COVID-19 patients and used for SARS-
943 CoV-2-specific IgG measurement. IgG responses against SARS-CoV-2 S1- and N-protein in
944 (A, C) critically (red symbols) and (B, D) severely (blue symbols) diseased patients. Dotted
945 lines represent cut-off values for commercial S1- and N- specific ELISA assays. Each symbol
946 represents the mean value of all samples which were available for each patient at the indicated
947 time range after symptom onset. There are no significant t-tests (i.e. p>0.05 for all
948 comparisons).
949

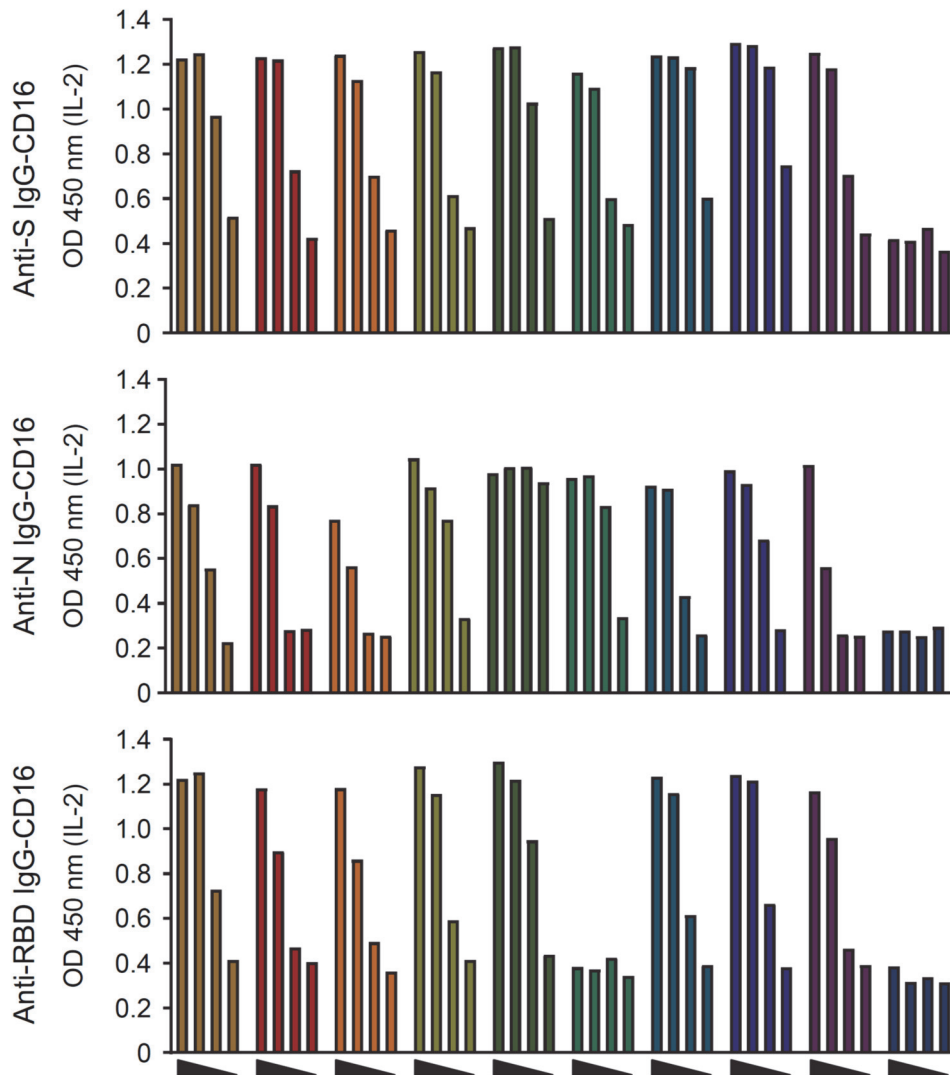
950 **Figure 2-figure supplement 1.**
951



952 **Cell-based reporter assay measuring CD16 activation in response to immobilized IgG and**
953 **sICs.**
954

955 BW5147 reporter cells expressing chimeric human Fc γ RIII secrete IL-2 in response to Fc γ R
956 activation by A) clustered viral specific IgG binding solid-phase antigen or B) soluble ICs.
957 Solubility of sICs is achieved by pre-blocking an ELISA plate with PBS supplemented with
958 10% FCS as previously described²⁵.
959

960 **Figure 2-figure supplement 2.**
961
962

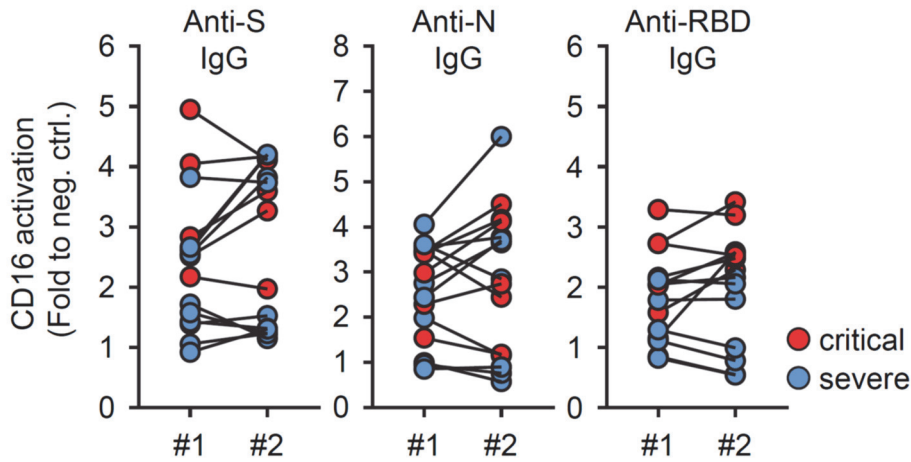


963
964
965
966
967
968
969
970
971
972
973

Dose dependent CD16 activation by SARS-CoV-2 specific IgG.

CD16 activation by A) S-, B) N- and C) RBD-specific IgG in 9 representatively selected serum samples and one SARS-CoV-2 negative serum (dark blue bars). Sera were serially diluted at 1:20, 1:100, 1:500 and 1:2500. Fc γ RIII activation initiates IL-2 secretion by reporter cells, which is subsequently measured via ELISA (OD 450 nm). Based on this empirical pretesting all sera were thereafter tested at 1:100 and 1:500 dilutions to reach an optimal dynamic range of response. The OD values obtained by the 1:500 dilutions were used for subsequent data analysis.

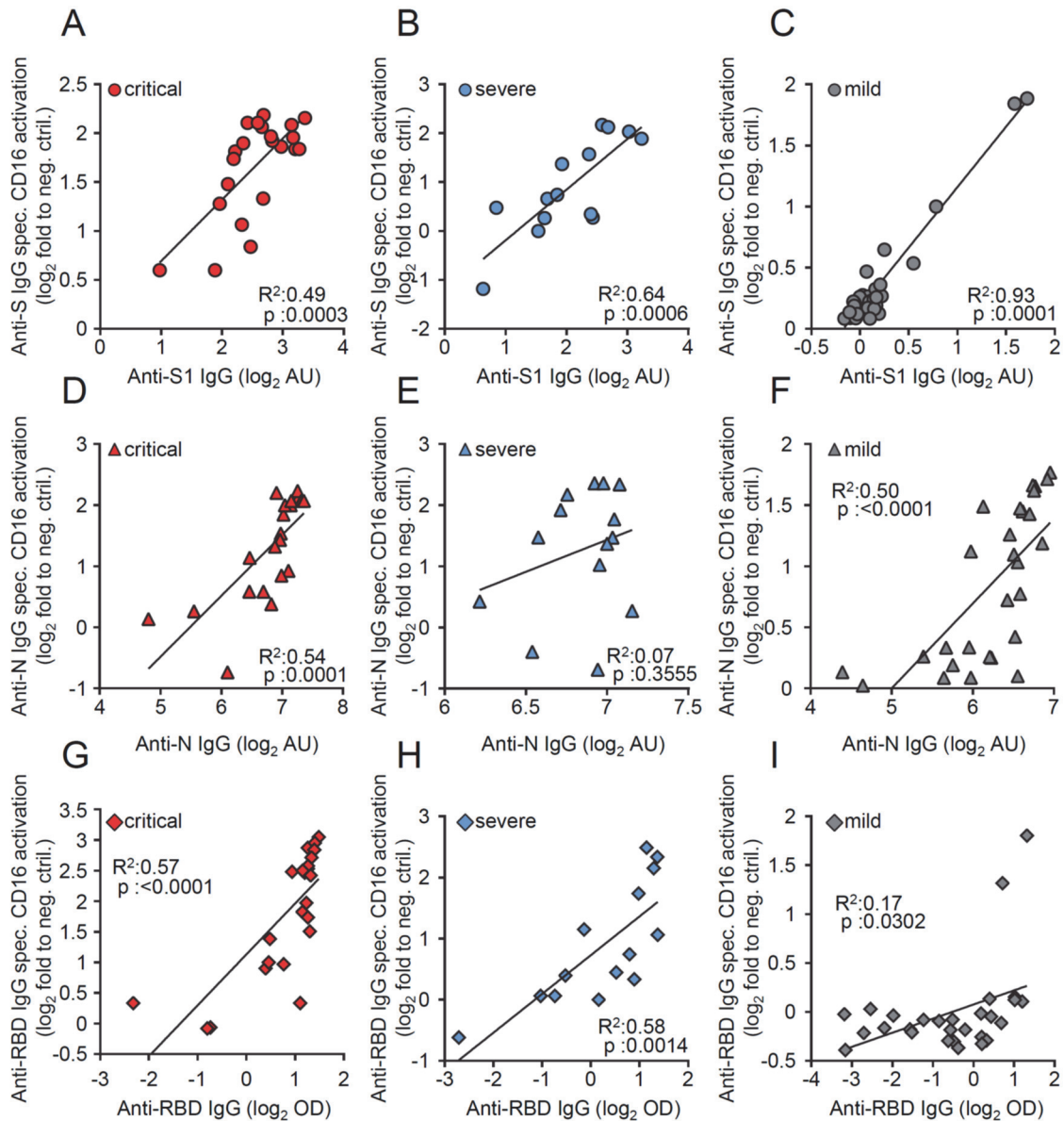
974 **Figure 2-figure supplement 3.**
975
976



977
978
979
980
981
982
983
984
985

Reproducibility of CD16 activation measurements by SARS-CoV-2 specific IgG. Selected sera which were available in sufficient amount from patients with critical (red symbols) or severe (blue symbols) SARS-CoV-2 infection were tested in two independent experiments to show reproducibility and consistency of results. CD16 activation by S-, N- and RBD specific IgG is shown. Statistical tests using a Kolmogorov-Smirnov test indicate no significant differences.

986 **Figure 2-figure supplement 4.**
987



988
989
990
991
992
993
994
995
996

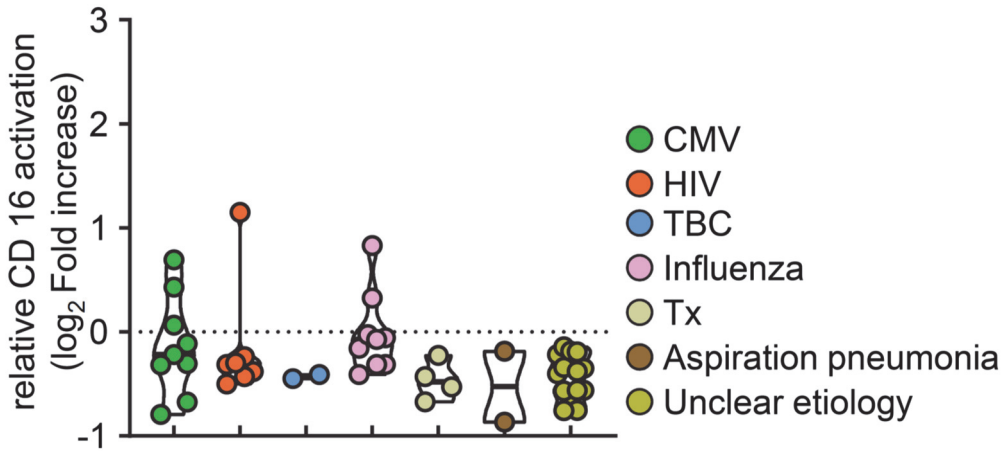
Correlation of CD16 activation by virus specific IgG and ELISA levels.

Pearson's correlation coefficient was used to assess the relationship between virus-specific IgG levels and their capability to trigger CD16 activation on BW5147 reporter cells in 22 paired samples from patients with critical disease (red symbols), 14 paired samples from patients with severe disease (blue symbols) and 28 samples from patients with mild disease (grey symbols). Each dot represents the mean value obtained by the analysis of all samples available at the indicated time points. (A-C) anti-S IgG, (D-F) anti-N IgG and anti-RBD-IgG (E-I).

997 **Figure 4-figure supplement 1.**

998

999



1000

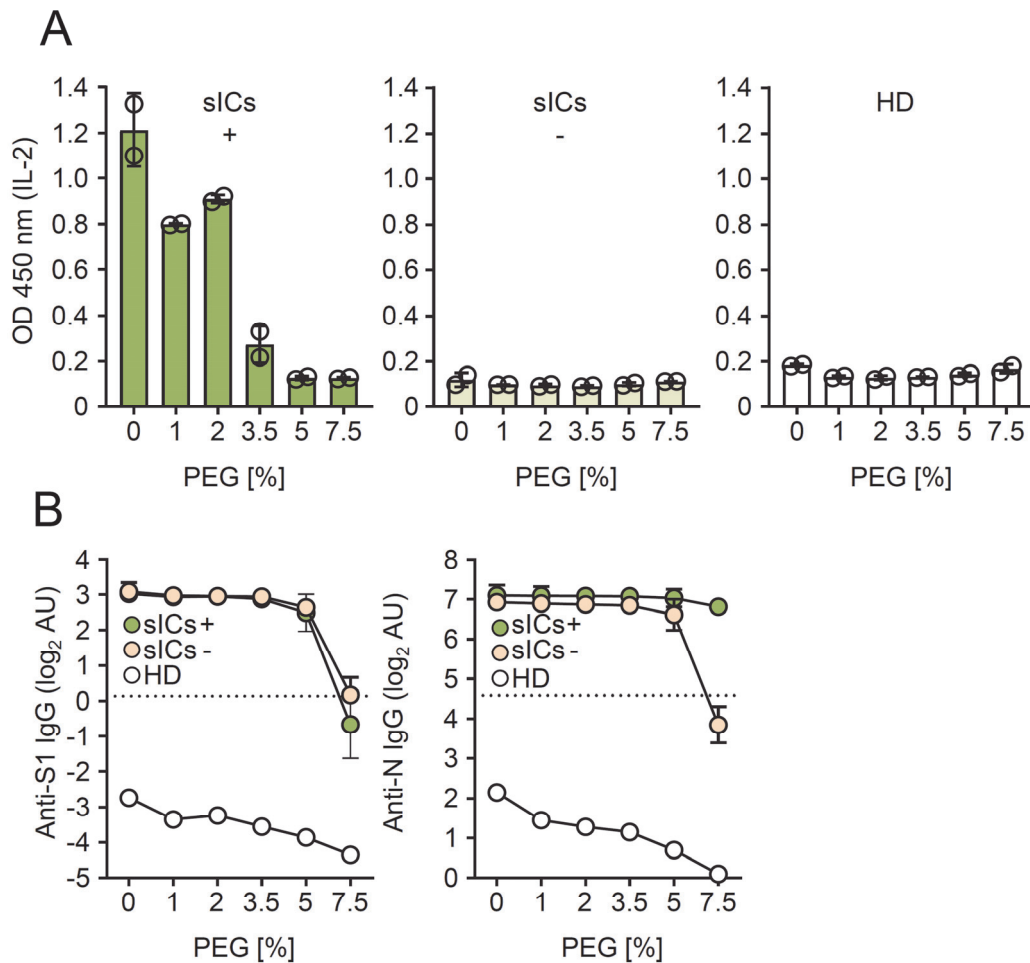
1001

1002 **CD16 activation by sICs in non-COVID-19 patients with ARDS.**

1003 Serum samples from 47 patients with ARDS in response to infections of different etiology were
1004 analyzed in a cell-based reporter assay which is sensitive to sIC amount and size²⁵. FcγR
1005 activation is shown as log₂ fold change relative to negative control. Each symbol represents one
1006 sample from one patient. CMV: Cytomegalovirus reactivation under immunosuppression; HIV:
1007 HIV infection; TBC: Mycobacterium tuberculosis infection; Influenza: influenza virus
1008 infection; TX: solid organ transplantation. Solid black lines indicate the median.

1009

1010 **Figure 4-figure supplement 2.**
1011

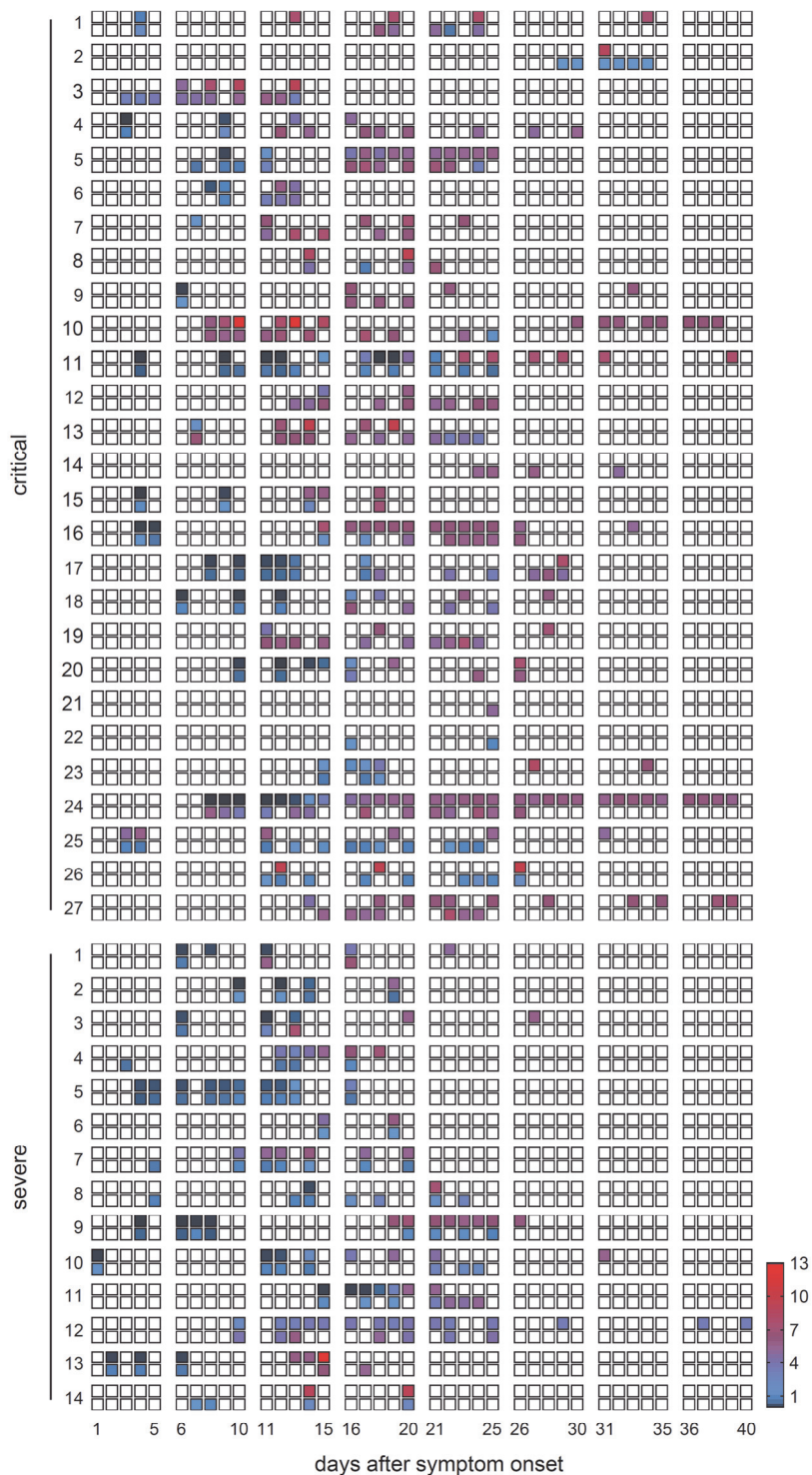


1012
1013

1014 **PEG precipitation eliminates sIC-mediated CD16 activation.**

1015 Pools of 8 sera were incubated with equal volumes of PEG8000 to reach the indicated final
1016 PEG concentrations. A) CD16 activation after PEG-precipitation in the pool supernatant,
1017 showing either high (sICs+) or no (sICs-) CD16 activation. Sera from healthy donors (HD)
1018 were included as a negative control. Activation levels are expressed as IL-2 levels (OD 450 nm)
1019 released by reporter cells. The mean and SD of two independent experiments is depicted. B)
1020 Anti SARS-CoV-2 IgG levels against S1 (left panel) or N (right panel) IgG following PEG
1021 precipitation. The mean and SD of two independent experiments (sICs+/sICs-) is depicted.
1022

1023 **Figure 4-figure supplement 3.**



1024

1025 **Individual CD16 activation by sICs and anti-S1 ELISA IgG kinetics post symptoms onset.**

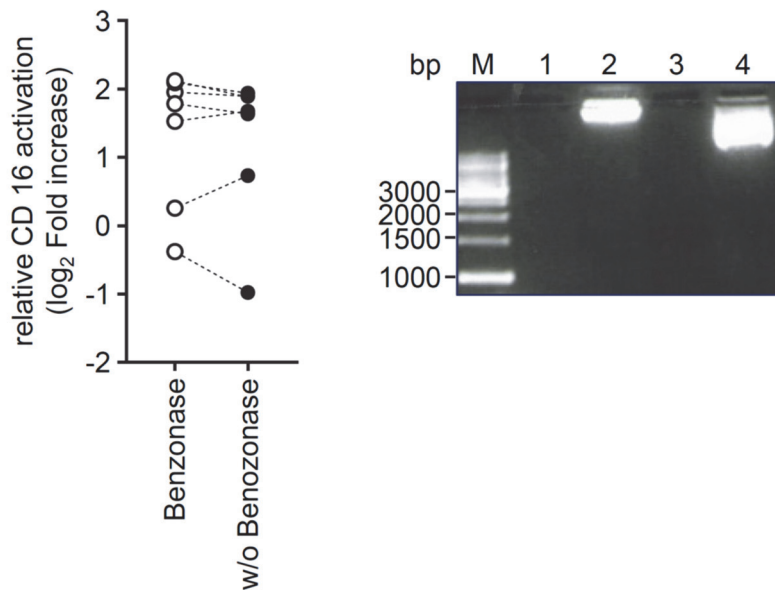
1026 Individual sera from either critically (n = 27) or severely (n = 14) diseased patients were
1027 analyzed via ELISA [AU] for anti S1-IgG (upper row) and for CD16 activation by soluble
1028 immune complexes (lower row, relative CD16 activation depicted as fold increase to the
1029 negative control) over time (1-40 days post symptom onset). White squares: not tested.
1030

1031

1032 **figure 4-figure supplement 4.**

1033

1034



1035

1036

1037 **Benzonase treatment of sIC-reactive sera does not abolish CD16 activation.**

1038 Left panel: sIC-mediated CD16 reactivity expressed as log₂ fold increase to the negative

1039 control, in serum of six individual patients before and after treatment with 250 Units of

1040 Benzonase Nuclease. Right panel: As positive control, 3 μ g plasmid DNA was digested. M:

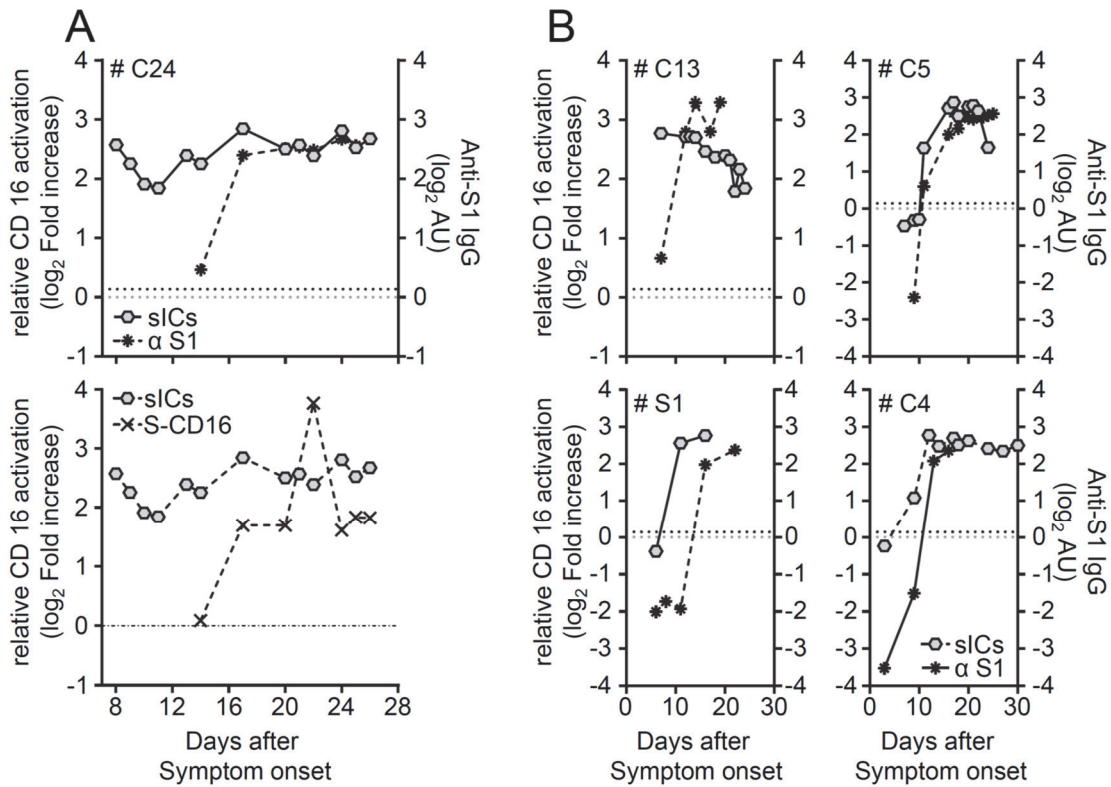
1041 1kb DNA ladder, Lane 1: benzonase digestion in the presence of human serum, lane 2: plasmid

1042 DNA w/o benzonase in the presence of human serum, lane 3: benzonase digestion in medium

1043 only and lane 4: plasmid DNA w/o benzonase in medium only.

1044

1045 **Figure 4-figure supplement 5.**
1046



1047
1048
1049
1050
1051
1052
1053
1054
1055
1056
1057

sICs formation precedes SARS-CoV-2-IgG response

Individual patients for which enough material was available were analyzed over time. A) CD16 activation by sICs- vs. S1-ELISA (top panel) and sIC –CD16 activation vs. anti-S- CD16 activation (bottom panel) in one critically ill patient, #C24. B) sIC-CD16 activation vs. S1-ELISA in four individual patients #C13, #C5, #S1 and #C4. Dashed line (black) represents commercial S1-ELISA-Cut-off level, whereas dashed line (grey) is set to 0. Individual longitudinal courses correspond to patients depicted in figure 4 supplement 3.